Available online at www.sciencedirect.com

SciVerse ScienceDirect

journal homepage: www.elsevier.com/locate/he

Review

Nanoscale and nano-structured electrodes of solid oxide fuel cells by infiltration: Advances and challenges

*San Ping Jiang**

Fuels and Energy Technology Institute, Department of Chemical Engineering, Curtin University, Perth, WA 6102, Australia

ARTICLE INFO

Article history:
Received 13 May 2011
Received in revised form
12 September 2011
Accepted 13 September 2011
Available online 14 October 2011

Keywords:
Solid oxide fuel cells
Review
Nano-structured electrodes
Infiltration
Electrocatalytic nanoparticles
Scaffold

ABSTRACT

Solid oxide fuel cells (SOFCs) are the most efficient devices for the direct conversion of the chemical energy stored in fuels such as hydrogen and hydrocarbons into electricity. The development of highly efficient and robust SOFCs requires cathodes and anodes with high electrocatalytic activity for O_2 reduction and direct oxidation of hydrocarbon fuels, respectively. Nanoscale engineering of electrode structures via metal salt solution impregnation or infiltration attracts increasing attention as the most effective way to develop highly active and advanced electrode structures for SOFCs. The infiltration method opens a new horizon in the advanced electrode development as the method expands the set of variable electrode materials combinations with the elimination of thermal expansion mismatch and the suppression of potential detrimental reactions between electrode and electrolyte materials. In this article, the advances and challenges in the development of nanoscale and nano-structured electrodes and the fundamental understanding of the remarkable enhancement in the electrode performance are reviewed and discussed with primary focus on the progress and status of the field in the last 5 years.

1. Introduction

The excessive and accelerated use of fossil fuels, especially coal, oil and gas, in the last 100 years has triggered a global energy crisis, and carbon dioxide emission from power generation burning fossil fuels is considered as a key contributor to climate change and related environmental problems. With increasing energy demand and depleting fossil fuel reserves, the current power generation from fossil fuels will not be sustainable.

Consequently, there are urgent needs to increase electricity generation efficiency and to develop renewable energy sources. Among the power generation technologies, fuel cell is considered to be the most efficient, clean power-generating technology, and is a potential and viable candidate to moderate the fast increase in power requirements and to minimize the impact of the increased power consumption on the environment. Fuel cells are electrochemical reactors in which the chemical energy contained in fuels such as hydrogen, methane, methanol, etc is converted directly into electricity. Fuel cells are inherently much more efficient than other existing energy conversion technologies such as internal combustion engines and there are significant interests worldwide in the development of fuel cells as environmental friendly and high efficient energy conversion technologies. Among various types of fuel cells, the two types that have received the most attention

* Tel.: +61 8 9266 9804.
E-mail address: s.jiang@curtin.edu.au.
0360-3199/$ – see front matter
doi:10.1016/j.ijhydene.2011.09.067

are the low temperature proton exchange membrane fuel cells (PEMFCs) and high temperature solid oxide fuel cells (SOFCs). PEMFCs systems use proton exchange polymer membranes as the electrolyte and precious platinum, palladium, ruthenium and/or their alloys as the electrocatalysts. Since Pt, Pd and Ru are precious metals, it is natural and logical that significant efforts have been made in the synthesis, development and optimization of Pt-based electrocatalysts to increase the Pt utilization via the nanoscale engineering and nanotechnologies [1]. SOFCs operate at temperature range of 600–1000 °C, promote rapid kinetics with non-precious materials and offer high fuel flexibilities. However, the nanoscale engineering and nano-structured approach in the development of high efficient and high performance electrodes in SOFCs and more recently in high temperature solid oxide electrolysis cells (SOECs) is relatively new phenomena, but the interest in this area grows very rapidly in the last 5–10 years.

A typical SOFC consists of a dense layer of an oxygen ion conducting electrolyte separating a cathode, on which oxygen molecules react with electrons to produce oxygen anions, from an anode on which the fuel is oxidized (see Fig. 1). The electrons that are produced during the oxidation of fuels are transported through an external load back to the cathode. In practice, the actual voltage of a fuel cell is less than the theoretical Nernst value due to the irreversible losses associated with transport of the ions through the electrolyte, finite rates of the electrode reactions and mass transport losses of gases in the porous electrodes. The electrolyte losses can be limited by using thin Y_2O_3-ZrO_2 (YSZ) electrolyte layers or alternative electrolyte materials such as doped ceria and $LaGaO_3$ [2–4]. It has been well known to the SOFC community that losses associated with the electrode processes can be minimized through carefully engineering and optimization of the three phase boundaries (TPBs) where electrode, electrolyte and gas phases meet. A well adopted strategy is to develop new cathode and anode materials with high electrochemical activity and stability for the electrode reaction with good tolerance toward impurities such as chromium in the case of metallic interconnect and carbon and sulfur in the case of hydrocarbon fuels. Despite the enormous efforts in the development of new electrode materials for SOFCs for the operating at intermediate temperatures of 500–800 °C (low operation temperature of IT-SOFCs has potential advantages of significantly increased materials section, reduced materials and fabrication cost and increased long-term stability [5]), challenges still remain; "Development of new electrode or electrolyte materials is not a straightforward and simple issue in SOFC and requires careful consideration of the compatibility and stability with various cell components. This is usually a long and costly process", as pointed out in 2006 [6]. Against this background, the new approach for the development of nano-structured electrodes by wet impregnation or infiltration has been gaining increased attention in the last few years. This paper will start with a brief overview of the anode and cathode in SOFCs and the emphasis will be on the progress and achievements in the development of nano-structured electrodes in SOFCs and most recently in SOECs in the last 5 years.

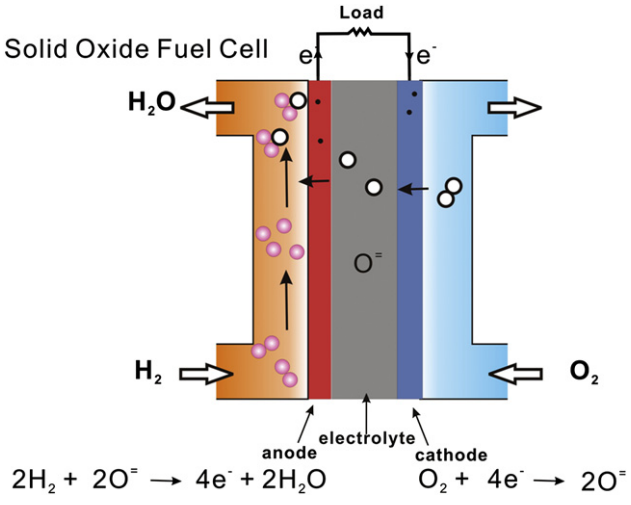

Fig. 1 – Schematic of operating principle of a solid oxide fuel cell.

2. An overview of current anodes and cathodes

A SOFC cathode is the material where pure oxygen or oxygen from air is reduced to oxygen ions through the combination of electrons externally from the cell, and the oxygen reduction reaction requires the presence of oxygen and electrons as well as the transportation of generated oxygen ions from the reaction sites to the bulk of the electrolyte. Thus, the materials used as the SOFC cathodes should have high electronic conductivity and oxygen ionic conductivity, and should also meet the requirement of chemical and thermal stability in oxidizing environment, chemical and thermal compatibility with the electrolyte, and high catalytic activity toward oxygen reduction reactions at intermediate temperatures. Similarly, the anode materials of SOFCs must have high electronic conductivity and oxygen ion conductivity, high activity for the oxidation reaction of fuels such as hydrogen, methane and light hydrocarbons as well as redox stability under oxidation environment. However, limited materials up to now have met the complete requirements for SOFC cathodes and anodes.

Strontium-doped lanthanum manganite (LSM) is the most common cathode materials for SOFC because of its high electrochemical activity for the O_2 reduction reaction at high temperatures, good thermal stability, good chemical stability and compatibility with the most commonly used YSZ electrolyte, and the demonstrated structural stability under SOFC operation conditions [7,8]. LSM is an excellent electronic conductor (its electronic conductivity is ~200 S cm^{-1} at 800 °C [9]), but with a negligible oxygen ionic conductivity (e.g., ~10^{-16} cm^2 s^{-1} at 700 °C) [10]. As the incorporation and bulk diffusion of oxygen inside LSM cannot be expected to occur to a significant degree, the O_2 reduction reaction is limited to TPB areas at the electrode/electrolyte interface. Thus, with the reduced operation temperature of SOFCs, the polarization resistance for the O_2 reduction reaction on the LSM-based cathodes increases significantly [11]. As a result, pure LSM is not a suitable candidate as the SOFC cathode at intermediate temperatures of 600–800 °C.

Various strategies have been developed to improve the electrocatalytic activity of the LSM-based cathodes. Murray

and Barnett [12,13] showed that the addition of YSZ and GDC to LSM significantly reduced the electrode polarization resistance. The electrode polarization resistance decreases as the GDC concentration increased to 50 wt%. Another family of materials that has been extensively studied for SOFC cathode is $LaCoO_3$-based perovskites. $LaCoO_3$, like $LaMnO_3$, shows *p*-type electronic conductivity. Acceptor-doped cobaltites are characterized by enhanced lattice oxygen vacancy formation and, hence high ionic conductivity. However, the thermal expansion coefficient (TEC) of Co-rich perovskites, $\sim 20 \times 10^{-6}\ K^{-1}$, is generally too high for both YSZ and doped CeO_2 electrolytes. An alternative to the Co-rich perovskites is the Sr-doped $LaFeO_3$ which has a lower TEC and a good chemical compatibility with doped CeO_2 electrolyte. Compositions in the system (La,Sr)(Co,Fe)O_3, such as $La_{0.6}Sr_{0.4}Co_{0.2}Fe_{0.8}O_3$ or LSCF6428 [14], may have desirable properties for IT-SOFC cathode applications. The oxygen self-diffusion coefficient of cobaltite based materials is several orders of magnitude higher than that of the manganites [10]. Maximum power density of 0.99 W cm^{-2} at 600 °C was achieved on a thin $Gd_{0.1}Ce_{0.9}O_{1.95}$ (GDC) electrolyte cell with nano-structured LSCF cathodes [15]. The addition of ionically conductive phase, such as GDC also promotes the electrocatalytic activity of LSCF cathodes [16–18].

Barium-based cobalt ferrite was also developed as cathodes of SOFCs. Shao and Haile [19] applied $Ba_{0.5}Sr_{0.5}Co_{0.8}Fe_{0.2}O_3$ (BSCF) as cathode to a doped ceria electrolyte cell and achieved the power densities of 1.01 W cm^{-2} and 402 mW cm^{-2} at 600 °C and 500 °C, respectively, when operated with hydrogen as the fuel and air as the oxidant. However, the TEC of BSCF is $\sim 20 \times 10^{-6}\ K^{-1}$ and the electronic conductivity is low, $\sim$25 S cm^{-1} at 800 °C [20]. The low conductivity of the BSCF is a serious concern in practical application in SOFCs as the low conductivity of the electrode materials would lead to the significant increase in the contact resistance between the current collector and the electrode, resulting in the increase in the electrode polarization losses [21]. The presence of CO_2 also deteriorates the BSCF performance by adsorbing on the cathode surface and thus obstructing the oxygen surface exchange reaction [22]. A number of other oxide materials have also been investigated as cathodes of SOFCs. Examples are lanthanum nickelate, $La_2NiO_{4+\delta}$ (LN) [23], La(Ni, M)O_3 (M = Al, Cr, Mn, Fe, Co, Ga) perovskites [24], lanthanum strontium manganese chromite, $La_{0.75}Sr_{0.25}Cr_{0.5}Mn_{0.5}O_3$ [25], and GdBaCoO_5 [26]. However, their long-term stability under SOFC operating conditions is generally unproven.

$La_{1-x}Sr_xMO_3$ (M = Co, Ni and Fe) and in general cobalt-based perovskites are not as stable as their manganite counterparts [27], though excellent performance and good stability have been reported for LSF based cathodes [28,29]. The preparation of lanthanum cobalt ferrite or nickelate perovskites is complicated by that fact they readily react with YSZ at the sintering temperatures required for the fabrication of standard SOFC electrodes [30–32]. The interaction between the nano-structured thin film cathodes of $La_{0.5}Sr_{0.5}CoO_3$ and YSZ could even occur at 650–700 °C [33]. Use of interlayer such as doped ceria can prevent the interaction, but the long-term stability of such double layer structure is largely unknown.

The state-of-the-art anode materials for the H_2 oxidation reaction are the Ni/YSZ cermets due to their high electronic conductivity, high electrochemical activity for the H_2 oxidation, high structural stability and compatibility with YSZ electrolyte [34]. The function of the oxide component is primarily to reduce the sintering of the Ni metal phase, to decrease the TEC and to improve the electrochemical performance of the anode. Thus, the composition and phase distribution are important for the electronic conductivity, microstructure and performance of the Ni-based anode. The YSZ phase in the cermet plays a significant role in the creation of additional reaction sites by extension of the TPB [35].

For hydrocarbon fuels such as natural gas, the most abundant impurity is sulfur, existing as gaseous hydrogen sulfide, H_2S, after reforming. Sulfur is a major impurity in coal, so sulfur tolerance is also a major issue for SOFC power plants designed to utilize gasified coal. Ni-based anodes have very low level tolerance toward the sulfur poisoning [36]. Nickel and alloys based metals also corrode in high carbon-activity gases by a process known as metal dusting. Metal dusting involves carbon deposition and incorporation into the metal that results in the disintegration of bulk metals and alloys into metal particles at high temperatures (300–850 °C). The carbon deposition/cracking on Ni/YSZ cermet anodes can be avoided by providing a high enough steam to carbon (S/C) ratio in the fuel gas, e.g., by mixing the fuel with H_2O [37]. However, high S/C ratio is not attractive for fuel cells as it lowers the electrical efficiency of the fuel cells by diluting the fuel. The endothermic nature of the steam reforming reaction can also cause local cooling and steep thermal gradients potentially capable of mechanically damaging the cell stack. Thus, development of anodes with high tolerance toward carbon deposition and sulfur poisoning is critical for SOFCs utilizing hydrocarbon fuels. A number of groups have shown that perovskite oxides, e.g., $(La_{0.75}Sr_{0.25})(Cr_{0.5}Mn_{0.5})O_3$ (LSCM) and (La,Sr)VO_3 (LSV), exhibit better sulfur tolerance [38–41]; LSV makes it possible to work with $\sim$10% H_2S in the fuel [40]. Unfortunately, LSV appears to be insufficiently stable for use in SOFCs.

Oxide materials based on perovskite-related structures have been extensively investigated as alternative anode for SOFCs. Examples include titanates-based perovskites [42], yttria-stabilized zirconia-terbia (YSZT) such as Y_2O_3-ZrO_2-TiO_2 and Sc_2O_3-Y_2O_3-ZrO_2-TiO_2 [43], perovskite $SrTiO_3$ doped with La or Nb and niobium based tetragonal tungsten bronzes [44,45], $La_{0.75}Sr_{0.25}Cr_{0.5}Mn_{0.5}O_3$ (LSCM) [46], and double perovskites $Sr_2Mg_{1-x}Mn_xMoO_{6-\delta}$ [47]. Among the perovskite-based materials, LSCM appears to be most promising. Tao and Irvine reported a maximum power density of 0.47 W cm^{-2} on a cell with LSCM anode and LSM cathode at 900 °C [46], which is considered to be compatible to the cell based on Ni/YSZ cermet anodes. However, the electronic conductivity of LSCM is very low, $\sim$0.22 S cm^{-1} in 10%H_2/N_2 [48]. The low electrical conductivity will result in the high ohmic losses and the high contact resistance between the electrode and current connector.

The nanoscale and nano-structured electrode approach by infiltration method attracts increasing attention as the viable alternative for the development of new electrodes for SOFCs. Infiltration method is a two-step sintering process, which effectively separate the catalytic active phase formation temperature from the sintering temperature as required to establish the intimate electrode/electrolyte interface bonding

in the standard SOFC electrodes. Due to the relatively low temperature for the formation of catalytic active phases, nano-size particles can be formed onto structurally stable and compatible scaffolds such as LSM, Ni/YSZ, and YSZ or doped ceria. The infiltration method opens a new horizon in the electrode development as the method expands the selection of variable electrode materials combinations with the minimized TEC mismatch and the suppression of possible detrimental reactions between electrode and electrolyte materials. Since the first review of the nano-structured electrodes via impregnation in 2006, [6] there has been significant progress in the development of nano-structured electrodes in SOFCs. This is indicated by the recent review articles on the nano-structured SOFC anodes [49] and cathodes [50–52].

3. Nano-structured electrodes – approach and status

3.1. *Deposition of nanoparticles by infiltration process*

Due to the fact that high process temperatures are required to achieve good bonding and contact between electrode and electrolyte, e.g., 1000–1150 °C for LSM cathodes and 1300–1400 °C for Ni/YSZ cermet anodes [53,54], the conventional approach to introduce nanoparticles in the green stage of the electrodes such as that commonly used in the development of Pt-based nano-structured electrocatalysts in PEMFCs is not very successful for the high temperature SOFC electrodes. Thus the key consideration in the development of nano-structured SOFC electrodes is to bypass the high processing temperature via the deposition of catalytically and/or electrochemically active nanoparticles into a rigid and pre-fired electronic and/or ionic conducting electrode or electrolyte scaffold/framework by infiltration techniques. An infiltration process involves the precipitation and decomposition of a metal salt solution inside a porous electrode or electrolyte structure. Fig. 2 shows schematically a typical synthesis route for the deposition of nano-sized particles into a pre-fired electrode or electrolyte scaffold or framework via infiltration of metal salt or nanoparticle suspension solutions. For example, wet infiltration of CeO_2 and Gd-doped CeO_2 (GDC) into pre-fired LSM cathode can be carried out by simply placing a drop of a $Ce(NO_3)_3$ or mixed $Gd(NO_3)_3$ and $Ce(NO_3)_3$ ($Gd_{0.2}Ce_{0.8}(NO_3)_x$) solution on top of the coating which

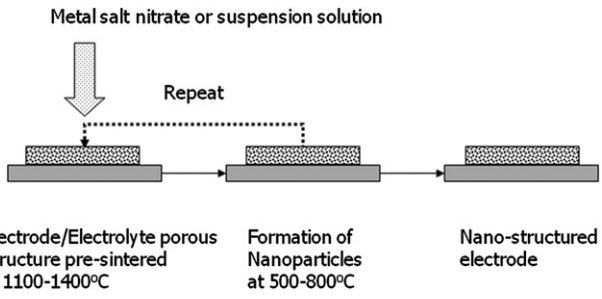

Fig. 2 – Typical process for the infiltration of metal salt nitrate solution or nanoparticle suspension into pre-sintered electrode or electrolyte porous structure.

infiltrates the cathode layer by capillary force. The infiltration process can be facilitated under vacuum [55]. Then the infiltrated LSM is heated at 500–800 °C to decompose the metal salt solution, forming CeO_2 or GDC nanoparticle phase. The phase formation temperature of the catalytic phase (i.e, CeO_2 or GDC) is much lower than the processing temperature of the standard LSM (i.e., ~1150 °C in this case). The significantly reduced phase formation temperature avoids the grain growth, resulting in the deposition of nano-sized GDC particles on the surface of grains of LSM scaffold.

The infiltrated catalytic nanoparticles can form discrete distribution or a thin and continuous network on the surface of the porous scaffold, as schematically shown in Fig. 3. The porous scaffold can be electronic conducting electrode materials such as LSM or ionic conducting electrolyte materials such as YSZ and doped ceria. The latter requires deposition of a continuous nanoparticle layer with high electronic conductivity as well as high electrocatalytic activity, and multiple infiltration steps are necessary to achieve sufficient electron conduction [56,57]. Such repeated infiltration process is time-consuming and hinders the practical application of the infiltration approach. Using a concentrated LSM nitrate precursor solution with surfactant (e.g., Triton-X100), Sholklapper et al showed that it may be possible to form a continuous and thin nano-structured LSM layer on YSZ scaffold with a single-step infiltration [52,58,59]. Fig. 4 shows a SEM picture of infiltrated LSM on porous YSZ scaffold [58]. The infiltrated LSM nanoparticles formed a continuous layer on YSZ grains with a thickness of 30–100 nm (~6 wt% of the YSZ scaffold). However, our own experience shows that in general it would be very difficult for concentrated precursor solutions to penetrate and infiltrate uniformly into micro- and nanopores of the scaffold by capillary force even under the vacuum treatment, and multiple infiltration-calcination steps are generally required, particularly in the case of thick anode-substrate supports.

Adding surfactants or complexing agents is beneficial for the uniform distribution and phase formation of infiltrated nanoparticles. Addition of urea and polymeric dispersant can facilitate the formation of perovskite phase such as $Sm_{0.6}Sr_{0.4}CoO_3$ and LSM at low temperatures [58,60], presumably due to the complexing effect of the additives. Addition of glycine is also shown to be effective to promote the uniform distribution of infiltrated yttria-stabilized bismuth (YSB) nanoparticles with reduced infiltration steps [61,62]. Li et al showed that the effect of adding urea is to enhance the distribution and electronic connectivity of Cu nanoparticle phases in the infiltrated Cu-YSZ composite anodes [63]. Nevertheless, the benefit of the additives appears to be related to the infiltrated nanoparticle phase and the scaffold. In a recent article, Nicholas and Barnett showed that adding additives such as surfactant Triton X-100 in $Sm_{0.5}Sr_{0.5}CoO_{3-x}$ (SSC) nitrite solution did not produce pure SSC phase while adding citric acid resulted in pure SSC phase. [64]. Furthermore, addition of additives such as Triton X-100 and citric acid had little effect on the morphology or the performance of the infiltrated SSC-GDC composite cathodes [64]. Electrodeposition and electroless deposition have also been used to accelerate the infiltration process [65,66]. However, the electrodeposition and electroless deposition

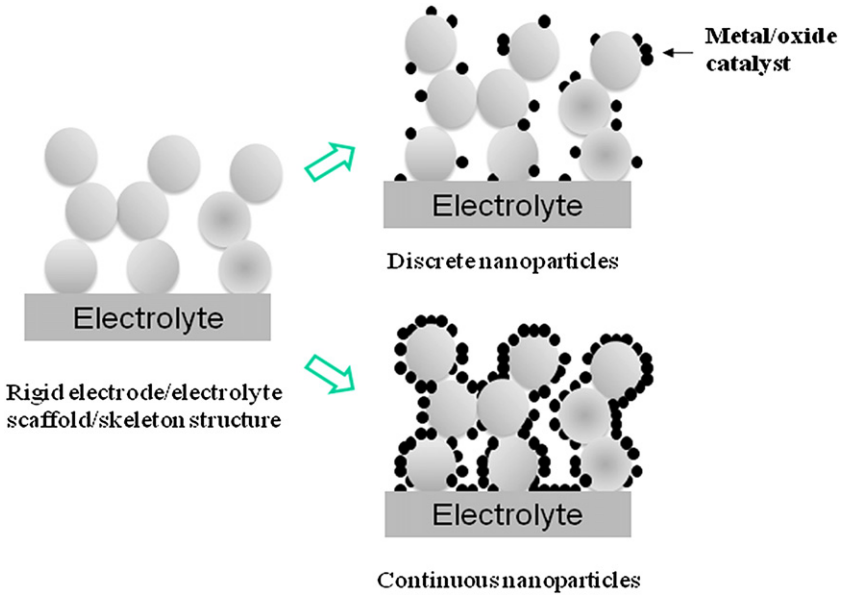

Fig. 3 – Scheme of the infiltrated nano-structured electrodes on pre-sintered porous electrode or electrolyte scaffold/skeleton.

require the porous scaffold to be conductive. Distribution of infiltrated nanoparticles also depends on the wetting properties between the metal salt solution and the porous scaffold. Lou et al shows that using SSC nitrate solution in a water/ethanol mixture significantly improves the wetting property between the infiltration solution and LSCF scaffold, resulting in the significantly enhanced SSC nanoparticle distribution and performance [67].

Cu-based anodes were initially developed for the direct oxidation of CH_4 [68]. Different to Ni, Cu is relatively inert for the formation of C–C bonds, however, its melting temperature is 1083 °C, significantly lower than 1453 °C for Ni. Therefore Cu-based cermet anodes cannot be produced using the same methods usually for Ni-based cermet anodes. The method developed by Prof. Gorte's group is to impregnate $Cu(NO_3)_2$ solution into porous YSZ scaffold prepared on a dense YSZ electrolyte layer, followed by calcinations to decompose the nitrate and form the oxide [69,70]. Both the dense electrolyte and porous scaffold can be fabricated by conventional tape-casting techniques, see Fig. 5 [50]. Other components such as ceria, perovskite oxides and precious metal catalysts can be added via infiltration processes to provide the ionic and electronic conductivity as well as the catalytic activity for the direct oxidation of hydrocarbons [71–79]. Similar to Cu-based anodes, silver with low melting temperature of 960 °C was also infiltrated into porous YSZ scaffold as potential anodes for hydrocarbon fuels, however, the activity of infiltrated Ag/YSZ composite anodes is not satisfactory, the area specific resistance, area specific resistance (ASR) is 38.4 Ωcm^2 in H_2 and 16.1 Ωcm^2 in CH_4 at 700 °C [80].

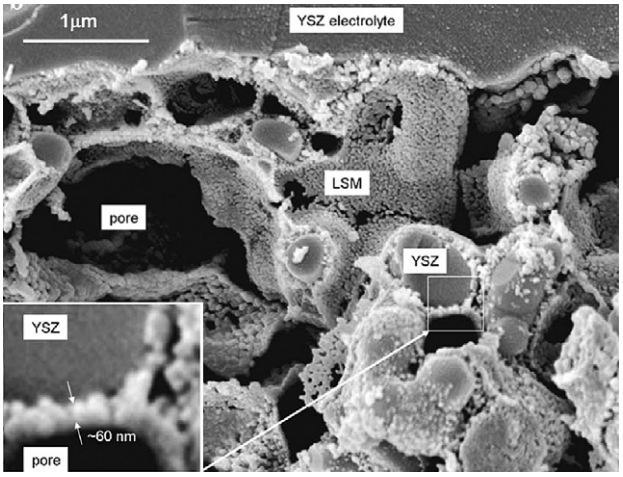

Fig. 4 – SEM micrograph of LSM infiltrated YSZ composite cathodes prepared from mixed nitrate solution with polymeric complexing agent, Triton X-100 [58].

3.2. *Performance of nano-structured electrodes*

Solution infiltration is extremely versatile in the development of wide range of nanostructures that combines the catalytic and electrochemical active phase with the structural rigidity of porous scaffold. Table 1 lists the performance and promotion factors of various nano-structured electrodes systems [55,56,81–99]. Recent development of nano-structured electrodes for SOEC [100,101] is also included in the Table. The promotion factor, f_P, was calculated by dividing the ASR (i.e., the electrode polarization resistance, R_E) or the overpotential, η of the nano-structured electrodes or power density of the cell with nano-structured electrodes by the performance of the baseline electrodes fabricated by conventional mixing and sintering processes, measured under identical conditions.

$$f_p = \mathrm{ASR}_{\text{infiltrated electrode}}/\mathrm{ASR}_{\text{conventional electrode}} \text{ or } \eta_{\text{infiltrated electrode}}/\eta_{\text{conventional electrode}} \quad (1)$$

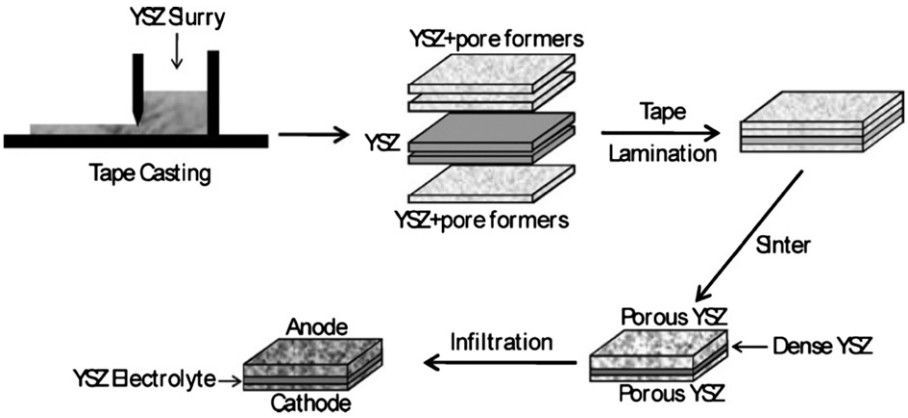

Fig. 5 – Diagram showing the steps used to fabricate an SOFC in which the electrodes are produced by infiltration of active components into a porous YSZ scaffold [50].

In addition to SOFCs and SOECs, infiltrated nano-structured electrodes have also been applied to metal-supported SOFCs and single-chamber SOFCs [102–104].

The enhancement in the electrochemical performance of nano-structured cathodes is truly remarkable. For instance, in the case of LSM cathodes, the electrode polarization (interface) resistance (R_E) is 11.7 Ωcm^2 at 700 °C. With the infiltration of 5.8 mg cm^{-2} GDC nanopartilces phase, R_E is reduced dramatically to 0.21 Ωcm^2 at 700 °C, which is 56 times smaller than that of the pure LSM cathode at the same temperature [105]. The R_E for the O_2 reduction reaction on the nano-structured Pd + YSZ is 0.11 Ωcm^2 at 750 °C and 0.22 Ωcm^2 at 700 °C, and this is

Table 1 – Performance and promotion factors of various nano-structured electrode systems.

Impregnated nanoparticles	Scaffold/skeleton	Performance	Promotion factor, f_P	Ref
Cathode of SOFC				
GDC (5.8 mg cm^{-2})	LSM	R_E = 0.21 Ωcm^2 @ 700 °C	56 for O_2 reduction	[81]
Pd (1.8 mg cm^{-2})	LSM/YSZ	R_E = 0.9 Ωcm^2 @ 600 °C	78 for O_2 reduction	[92]
Pd (1.2 mg cm^{-2})	LSCF	R_E = 2.9 Ωcm^2 @ 600 °C	1.9 for O_2 reduction	[90]
GDC (1.5 mg cm^{-2})	LSCF	R_E = 1.6 Ωcm^2 @ 600 °C	3.4 for O_2 reduction	[90]
LSM (~2 mg cm^{-2})	YSZ	R_E = 1.6 Ωcm^2 @ 600 °C	44 for O_2 reduction[a]	[92]
LSCF (1.1 mg cm^{-2})	YSZ	R_E = 0.54 Ωcm^2 @ 600 °C		[86]
LSCF (12.5 vol%)	GDC	R_E = 0.25 Ωcm^2 @ 600 °C	14 for O_2 reduction	[96]
$La_{0.6}Sr_{0.4}CoO_3$ (30 vol%)	YSZ	P = 2.1 W cm^{-2} @ 800 °C in H_2/air		[97]
$La_{0.6}Sr_{0.4}CoO_3$ (55 wt%)	SDC	R_E = 0.36 Ωcm^2 @ 600 °C		[93]
Ag	LSCF/GDC	P = 0.98 W cm^{-2} @ 600 °C	3.3 for H_2/air	[94]
Pd (1.4 mg cm^{-2})	YSZ	R_E = 0.22 Ωcm^2 @ 700 °C		[56]
BSCF (1.8 mg cm^{-2})	LSM	R_E = 1.3 Ωcm^2 @ 700 °C	12 for O_2 reduction	[89]
$Sm_{0.6}Sr_{0.4}CoO_3$	LSM/YSZ	R_E = 8.5 Ωcm^2 @ 600 °C	2.3 for O_2 reduction	[60]
$Y_{0.5}Bi_{1.5}O_3$ (50 wt%)	LSM	R_E = 0.14 Ωcm^2 @ 700 °C		[98,99]
Anode of SOFC				
$Sm_{0.2}Ce_{0.8}O_2$ (~4 mg cm^{-2})	Ni/YSZ	R_E = 0.24 Ωcm^2 @ 800 °C	7.3 for H_2 oxidation	[55]
GDC (4 mg cm^{-2})	$(La_{0.75}Sr_{0.25})(Cr_{0.5}Mn_{0.5})O_3$	R_E = 0.44 Ωcm^2 @ 800 °C	26 for CH_4 oxidation	[83]
GDC (4 mg cm^{-2})	$(La_{0.75}Sr_{0.25})(Cr_{0.5}Mn_{0.5})O_3$	R_E = 0.12 Ωcm^2 @ 800 °C	20 for H_2 oxidation	[83]
GDC (1.42 mg cm^{-2})	Ni	R_E = 1.29 Ωcm^2 @ 800 °C	25 for CH_4 oxidation	[84]
Pd (0.36–0.46 mg cm^{-2})	$(La_{0.75}Sr_{0.25})(Cr_{0.5}Mn_{0.5})O_3$/YSZ	R_E = 0.88 Ωcm^2 @ 800 °C	1.5 for H_2 oxidation	[85]
Pd (0.36–0.46 mg cm^{-2})	$(La_{0.75}Sr_{0.25})(Cr_{0.5}Mn_{0.5})O_3$/YSZ	R_E = 2.0 Ωcm^2 @ 800 °C	4.6 for CH_4 oxidation	[85,87]
Pd (0.36–0.46 mg cm^{-2})	$(La_{0.75}Sr_{0.25})(Cr_{0.5}Mn_{0.5})O_3$/YSZ	P = 0.111 W cm^{-2} @ 800 °C	8 for C_2H_5OH/air	[85]
Pd (0.06 mg cm^{-2})	$(La_{0.7}Ca_{0.3})(Cr_{0.5}Mn_{0.5})O_3$/GDC	R_E = 1.1 Ωcm^2 @ 750 °C	6.5 for CH_4 oxidation	[88]
Pd (0.11 mg cm^{-2})	Ni/GDC	R_E = 0.6 Ωcm^2 @ 700 °C	~5 for H_2 oxidation	[91]
Pd (5 wt%) + CeO_2 (5 wt%)	$(La_{0.75}Sr_{0.25})(Cr_{0.5}Mn_{0.5})O_3$/YSZ	P = 0.52 W cm^{-2} @ 700 °C	~5 for H_2/air	[95]
Oxygen electrode of SOEC				
GDC (2 mg cm^{-2})	LSM	R_E = 0.15 Ωcm^2 @ 800 °C[b]	148 for O_2 oxidation	[100]
LSM	YSZ	R_E = 0.48 Ωcm^2 @ 800 °C[c]	2.3 with 50% AH[c]	[101]

a Calculated based on performance for LSM/YSZ composite cathodes.
b Measured after polarized at 1000 mA cm^{-2}, 800 °C for 22 h.
c Measured on a SOEC with 50% absolute humidity (AH) and based on performance for LSM/YSZ oxygen electrode.

significantly lower than that of the LSM (9–54 Ωcm^2 at 700 °C [13,106]), LSM/YSZ (2.5 Ωcm^2 at 700 °C [12]) and LSM/GDC (1.1 Ωcm^2 at 700 °C [13]) composite cathodes.

The most distinctive advantage of the nano-structured approach is the flexibility in the selection and combination of highly active catalytic materials with structurally stable and highly electronic or ionic conducting scaffold to meet stringent requirements of anodes and cathodes of SOFCs. For example, the high performance SOFC cathodes required for anode-supported YSZ electrolyte cells can be fulfilled by the combination of highly active MIEC but thermally incompatible materials such as BSCF with the structurally stable and highly conductive LSM scaffold. In such nano-structured BSCF-infiltrated LSM composite cathode, the uniformly distributed BSCF nanoparticles significantly enhance the electrochemical activity, while the LSM scaffold provides an effective electron transfer path, TEC matching and thermal stability with the YSZ electrolyte. The interfacial reaction between the infiltrated BSCF and YSZ is minimized due to the low phase formation temperature of BSCF. Fig. 6 shows the performance of anode-supported YSZ film cells with pure LSM and 1.1 mg cm^{-2} BSCF-infiltrated LSM cathodes at different temperatures under H_2/air [89]. The cell with thin YSZ electrolyte film and the nano-structured BSCF-LSM cathode

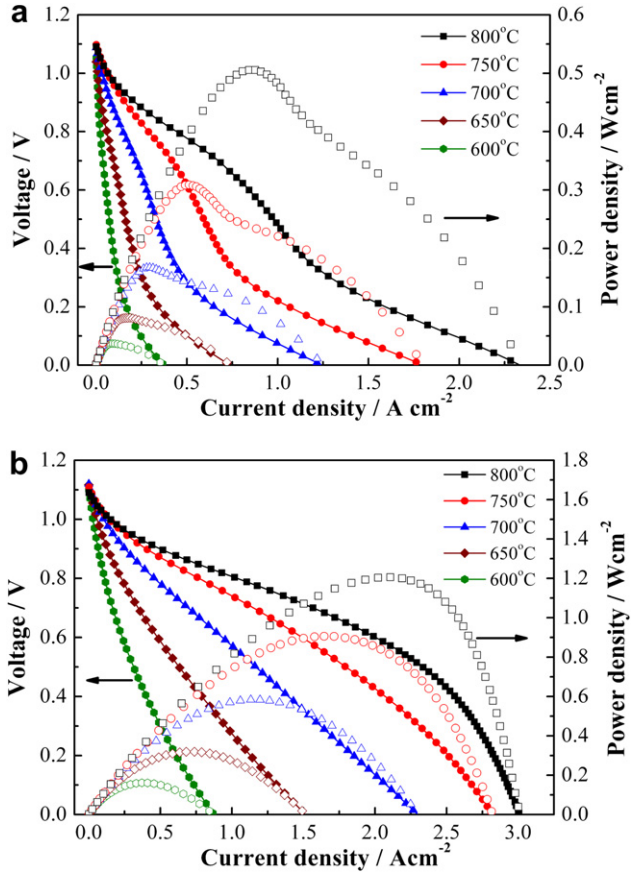

Fig. 6 – Performance of the Ni/YSZ anode-supported YSZ electrolyte film cells with (a) pure LSM cathode and (b) 1.1 mg cm^{-2} BSCF-infiltrated LSM composite cathode at different temperatures in H_2/air. H_2 flow rate: 200 mL min^{-1}; oxidant: stationary air [89].

exhibits maximum power densities of 1.21 and 0.32 W cm^{-2} at 800 °C and 650 °C, respectively, substantially higher than 0.51 and 0.08 W cm^{-2} for the cells with the pure LSM cathode under identical conditions. Highly active cobaltite based pervoskite cathodes such as $Sm_{0.5}Sr_{0.5}CoO_{3-\delta}$ (SSC), $La_{0.6}Sr_{0.4}CoO_{3-\delta}$ (LSC), $La_{0.8}Sr_{0.2}FeO_3$ (LSF), and LSCF, and K_2NiF_4-type materials such as $La_{n+1}Ni_nO_{3n+1}$ are also developed with YSZ electrolytes via infiltration route using porous SDC or YSZ scaffolds [57,86,107–111].

The promotion effect of infiltrated nanoparticles on the performance of nano-structured anodes is equally impressive. Replacing Ni with carbon-inert Cu to form Cu/YSZ cermet anodes [111] and infiltration of porous YSZ scaffold with copper, nickel and cerium nitrate solution [112] were found to improve significantly the resistance toward carbon deposition. Infiltration of catalytic active nanoparticles can substantially enhance the electrocatalytic activity of Ni-based cermet anodes as well as ceramic oxide anodes such as LSCM in H_2 and methane and suppress carbon deposition [55,83,84,113]. In the case of LSCM anodes, for example, the conductivity of LSCM is low, ~29 S cm^{-1} in air and 0.22 S cm^{-1} in 10% H_2 at 800 °C [48]. Our studies on LSCM-based electrodes show that the electrocatalytic activity of LSCM is also low in methane [114]. Introduction of GDC or Pd nanoparticles by infiltration substantially enhances the activity of LSCM anodes for the electrochemical oxidation reaction in H_2, CH_4 and C_2H_5OH fuels [83,85]. Fig. 7 shows the V–I curves and cell performance of LSCM, LSCM/YSZ, GDC- or Pd-infiltrated LSCM and LSCM/YSZ composite anodes. Pure LSCM and LSCM/YSZ composites have very poor electrocatalytic activities for the oxidation reaction of H_2, CH_4 and C_2H_5OH. With the infiltration of GDC or Pd nanoparticles, the electrocatalytic activity of the LSCM and LSCM/YSZ anodes is increased remarkably. GDC nanoparticles are equally effective for the promotion of the oxidation reaction of H_2 and CH_4 (Fig. 7a and b). However, the effect of the infiltrated Pd nanoparticles is most pronounced for the reaction in methane and ethanol. The maximum power output is 24 mW cm^{-2} for the cell with a pure LSCM/YSZ composite anode in CH_4 and is almost doubled to 45 mW cm^{-2} with the infiltration of ~0.4 mg cm^{-2} Pd nanoparticles (Fig. 7c). For the ethanol oxidation reaction on a pure LSCM/YSZ anode, the cell power density is only 14 mW cm^{-2}. After the infiltration of ~0.4 mg cm^{-2} Pd nanoparticles, the power density reaches 111 mW cm^{-2}, an 8-times increase in power output (Fig. 7d).

High temperature solid oxide electrolysis cell (SOEC) has a great potential for efficient and economic production of hydrogen fuel as it involves less electrical energy consumption compared to conventional low temperature water electrolysis [115]. SOEC is a reversely operated SOFC in which steam is fed to the cathode side of the SOEC where it is reduced to hydrogen. At the anode side, the oxygen ions immigrated from the electrolyte are oxidized to oxygen gas. The materials and fabrication technologies that are used for SOFCs can be directly applicable for SOECs. LSM is so far the most commonly used anode or oxygen electrode for SOECs. As shown recently by Elangovan et al. [116] one of the major problems for the long-term stability of the SOEC stacks is the degradation of the LSM-based electrodes due to the high oxygen partial pressure generated at the LSM/YSZ interface

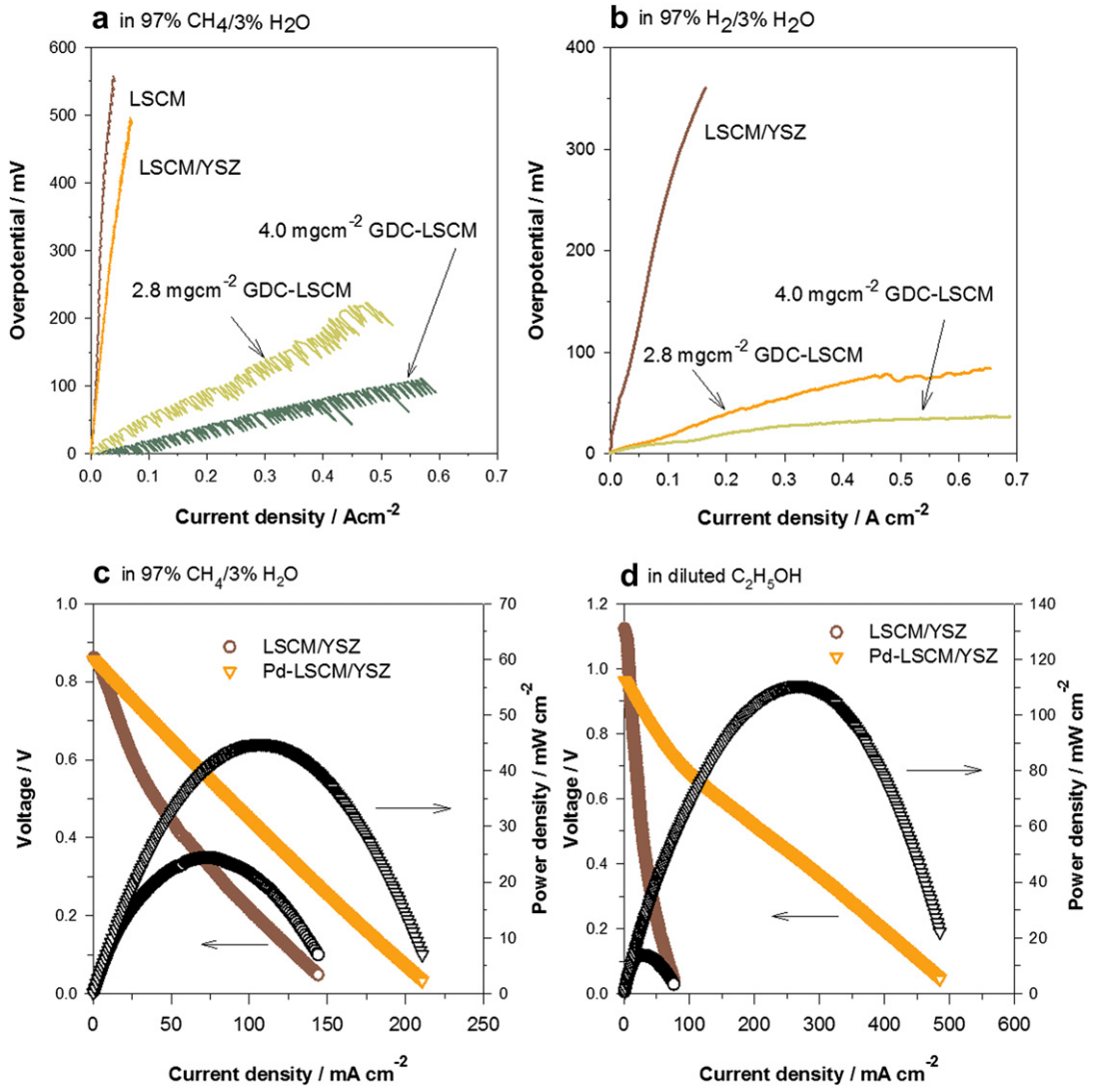

Fig. 7 – (a,b) Overpotential – current curves of LSCM, LSCM/YSZ and GDC-infiltrated LSCM anodes at 800 °C in wet CH_4 and H_2 and (c,d) performance of cells with and without ~0.4 mg cm^{-2} Pd-infiltrated LSCM/YSZ anodes at 800 °C in CH_4 and C_2H_5OH. The YSZ electrolyte thickness was 1 mm [83,85].

which causes the delamination of the oxygen electrodes. Recent study on the nano-structured GDC-infiltrated LSM oxygen electrodes at 800 °C showed that the introduction of the GDC nanoparticles phase not only leads to the enhanced electrocatalytic activities of the LSM oxygen electrode but also effectively inhibits the shrinkage and delamination of the LSM oxygen electrode under high anodic current polarization, significantly enhancing the stability and durability of the oxygen electrodes [100]. Nano-structured LSM-infiltrated YSZ oxygen electrodes also show significantly better performance as compared to conventional LSM/YSZ composite oxygen electrodes of SOECs [101].

3.3. *Microstructure of nano-structured electrodes*

The remarkable promotion effect of the nano-structured electrodes on the performance of anodes and cathodes of SOFCs is a direct result of the formation and uniform deposition of nano-sized and catalytically active phases on the surface of porous electrode or electrolyte scaffolds. Fig. 8 shows typical microstructures of selected nano-structured cathodes [117,118]. The GDC nanoparticles phase is formed after heat-treatment at 800 °C and the particle size is in the range of ~50 nm, which is much smaller than 1000–1500 nm of the LSM grains of the pre-sintered LSM electrode scaffold (Fig. 8a). LSM can also be infiltrated into pre-sintered YSZ electrolyte scaffold to form nano-structured LSM + YSZ composite cathodes (Fig. 8b). The infiltrated LSM phase is characterized by the formation of continuous LSM nano-particles on the surface of YSZ grains. The formation of continuous Pd nanoparticles on the YSZ grain surface via simple palladium nitrate solution infiltration process is clearly demonstrated by the SEM and high resolution TEM pictures of a Pd-infiltrated YSZ cathode (Fig. 8c and d). The Pd nano-particles are well interconnected. However, infiltrated Pd intends to form discrete nanoparticles on the surface of the

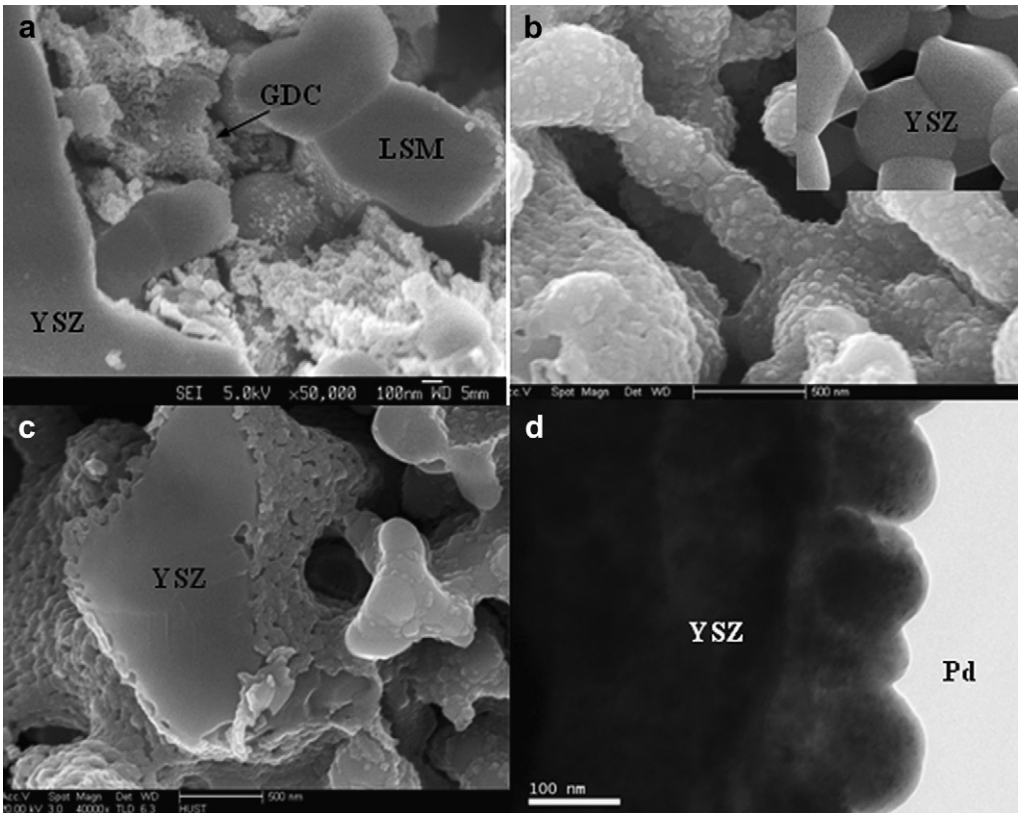

Fig. 8 – SEM micrographs of (a) GDC-infiltrated LSM, (b) LSM-infiltrated YSZ, (c) Pd-infiltrated YSZ, and (d) high resolution TEM of (c) [117,118]. The inset in (b) is the YSZ scaffold before infiltration.

anodes such as LSCM/YSZ and Ni/GDC under reducing environment [87,91,119].

One of the most important conclusions from the observed formation of continuous nanoparticles layers on highly porous YSZ scaffold (Fig. 8b and c) is that the resulting structure is not entirely random. Such characteristic is particularly important to achieve sufficient conductivity on the dominant ionic electrolyte scaffold structure using perovskite loadings below the normal percolation threshold of 30 vol% [50]. It has been shown that the conductivity of the infiltrated LSM + YSZ composite cathodes increases at very low LSM loading and threshold for the reasonable conductivity is below 20 vol%, significantly lower than the minimum value of 30 vol% based on the percolation theory for conventional LSM/YSZ composites [120]. The advantage of the electrolyte scaffold in the development of nano-structured electrodes is the better mechanical strength of the porous scaffold as compared to that of the electrode scaffold.

The intrinsic relationship between the microstructure of the nano-structured electrodes and the performance is further demonstrated in Fig. 9 [117]. The anode-supported cell with infiltrated nano-structured LSM-YSZ cathode (electrode II) achieved a power density of 0.83 W cm^{-2} at 750 °C in H_2/air, more than 4 times higher than that on similar cells with conventional LSM-YSZ composite cathode (electrode I). With the infiltration of Pd to conventional LSM-YSZ composite cathode (electrode III), the cell performance was enhanced substantially to 1.42 W cm^{-2}. Though the microstructure of LSM-infiltrated YSZ (LSM + YSZ) and Pd-infiltrated LSM-YSZ (Pd + LSM-YSZ) composite electrodes appears similar (Fig. 9b), the reaction paths on the electrode II and III are in fact very different. For electrode II, YSZ scaffold only provides the path for the oxygen ion conductivity and infiltrated LSM nanoparticles on YSZ surface provides the TPB for the O_2 reduction. In the case of nano-structured Pd + LSM-YSZ (electrode III), the LSM-YSZ scaffold is both electronic and ionic conductive and the deposition of Pd nanoparticles layers on the surface of the LSM-YSZ scaffold not only provides the additional reaction sites but also significantly accelerate the reaction rate of the dissociation and diffusion of oxygen species (Fig. 9a). This explains the very high performance of the cell with nano-structured Pd + LSM-YSZ composite cathodes.

Fig. 10 is the typical microstructures of selected nano-structured anodes [85,113]. Infiltrated GDC forms flow-like nanoparticle agglomerates on the Ni grain surface (Fig. 10a) while on the LSCM grain surface, a continuous GDC nanoparticle is formed with some agglomeration (Fig. 10b). The formation of agglomerates may be related to the poor wettability between the infiltration solution and the pre-sintered scaffold structures, as shown by Lou et al recently [67]. Pd forms discrete nanoparticles on the surface of the LSCM/YSZ composite anodes and initial particle size is in the range of 10–20 nm (Fig. 10c). After polarization test in wet CH_4 at 800 °C, Pd nanoparticles aggregate, forming relatively large Pd nanoparticles of 70–90 nm (Fig. 10d) [87]. This shows that the stability of the impregnated metal nanoparticles is still a major concern due to the inevitable agglomeration and grain

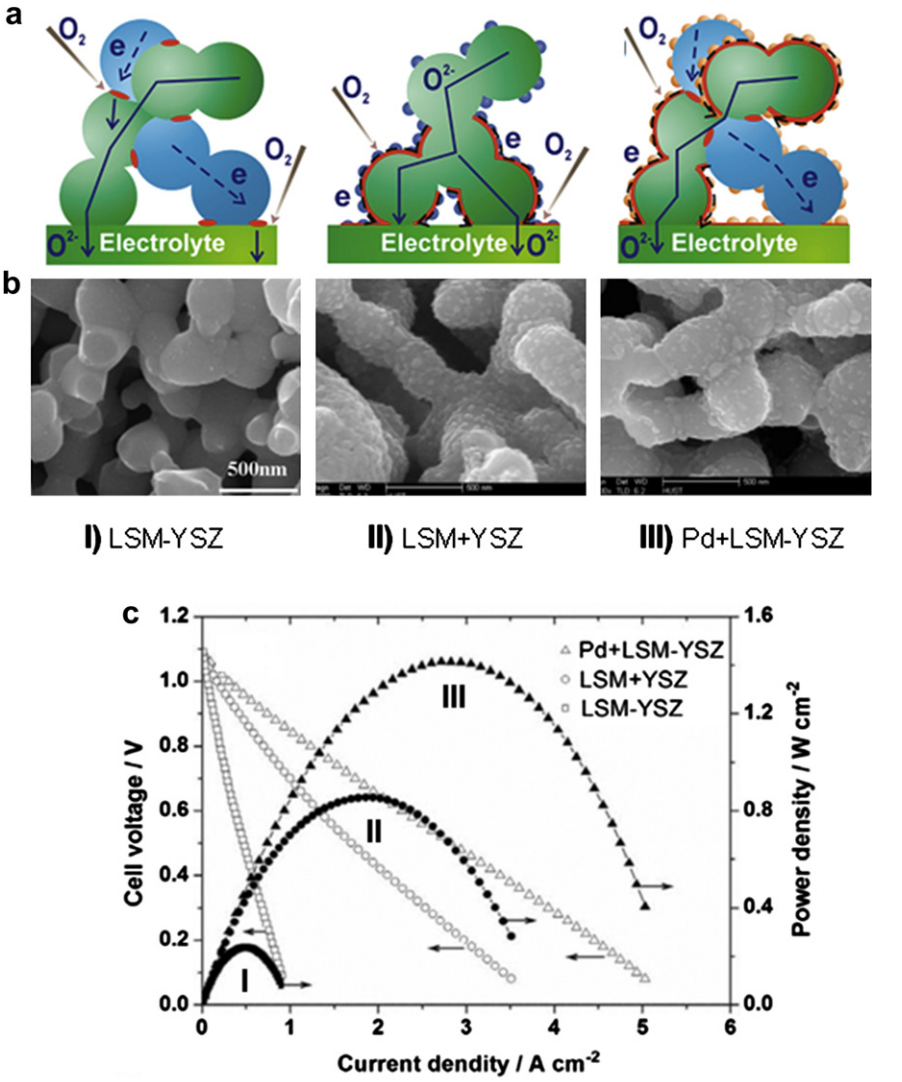

Fig. 9 – Demonstration of the performance and microstructure of the nano-structure electrodes. a) Schematic illustrations of electrodes I, II, and III, showing the paths of transport for electrons and oxygen ions and reaction sites for the O_2 reduction reaction; b) SEM micrographs of electrodes I, II, and III; c) Power output of anode-supported cells with electrode types I, II, and II, measured at 750 °C in H_2/air. Electrodes: (I) standard LSM-YSZ composite cathode by mechanical mixing of LSM and YSZ phases; (II) nano-structured LSM-infiltrated YSZ (LSM + YSZ) composite cathode; and (III) nano-structured Pd-infiltrated LSM-YSZ (Pd+LSM-YSZ) composite cathode [117].

growth of the nanoparticles under the high operation temperature of SOFCs.

The microstructure such as porosity and surface area of the porous scaffold also play an important role in the microstructure development and optimization of infiltrated electrodes. Shah and Barnett studied the relationship between the performance of LSCF infiltrated GDC composite cathode and the sintering temperature of GDC scaffold [96]. Increasing the GDC scaffold sintering temperature from 1000 to 1100 °C effectively decreases ASR due to the improved interconnectivity between GDC particles, however, increasing the sintering temperature above 1300 °C substantially increases ASR, most likely due to the decreased porosity. Organic or polymeric pore formers were used to control the scaffold pore size and the results show the impact of the pore size on the ASR of the infiltrated LSC-YSZ cathodes [107] and infiltrated Cu-ceria-YSZ anodes [121]. Other methods to control the microstructure of scaffold are also effective. For example, Armstrong and Rich fabricated YSZ scaffold from NiO-YSZ composites where the NiO was removed by reduction and subsequent acid leaching [97]. The advantage of this approach is to allow high sintering temperature and at the same time to retain the high surface area of the scaffold. Recent results by Küngas et al showed that treatment of YSZ scaffold with hydrofluoric acid (HF) can significantly increase the surface of YSZ scaffold and improve the performance of the infiltrated LSF cathodes [122].

Kim et al studied the effect of infiltrated Pd on the $(La_{0.75}Sr_{0.25})(Cr_{0.5}Mn_{0.5})O_3$ (LSCM)/YSZ composite anodes for the H_2 oxidation reaction [95]. LSCM/YSZ composite anodes

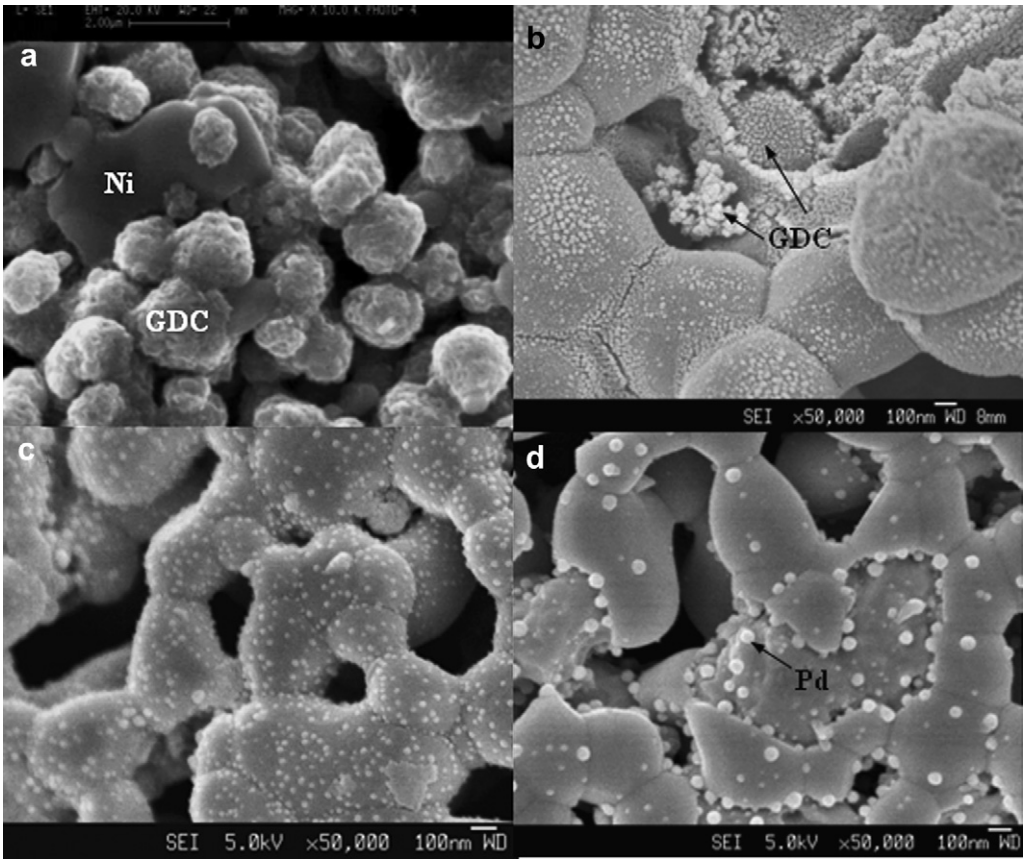

Fig. 10 – SEM micrographs of (a) GDC-infiltrated Ni, (b) GDC-infiltrated LSCM, (c) Pd-infiltrated LSCM/YSZ, and (d) Pd-infiltrated LSCM/YSZ anodes after polarization test [85,113].

were prepared by infiltrating YSZ scaffold with LSCM aqueous nitrate solutions, followed by sintering at 1200 °C. For pure LSCM/YSZ composite anodes, the maximum power density was 105 mW cm^{-2} in H_2 at 700 °C and increased significantly to 500 mW cm^{-2} with infiltration of ~0.5 wt% Pd. We also studied the effect of infiltrated Pd on the LSCM/YSZ composite anodes prepared by conventional method of sintering the mixed LSCM and YSZ oxides [85]. In the case of H_2, infiltration of ~0.46 wt% Pd had no significant effect on the cell performance. Fig. 11 compares the cell performance of the infiltrated Pd on infiltrated LSCM/YSZ anodes and on conventional LSCM/YSZ anodes [85,95]. The apparently significant differences in the promotion effect of infiltrated Pd on the LSCM/YSZ composite anodes for the H_2 oxidation may be related to the significant differences in the morphology of the scaffold of LSCM/YSZ composites prepared by infiltration and by conventional methods. As shown in Fig. 11c, after reduction in H_2, the infiltrated LSCM film is broken into very small particles and is highly porous [95]. This may imply that Pd may be able to infiltrate to the interface between the YSZ and LSCM, promoting the electrochemical reaction at the interface regions. In the case of conventional LSCM/YSZ composites, infiltrated Pd intends to form isolated nanoparticles on the surface of the LSCM or YSZ grains (see Fig. 10d). Thus, the morphology and microstructure of scaffold could also affect the distribution and thus the catalytic activity of the infiltrated nanoparticles.

4. Understanding the microstructural and catalytic effects of infiltrated nanoparticles

The peculiar microstructure of infiltrated nano-structured electrodes as shown in Figs. 4, 8 and 10 suggests the significantly enlarged TPBs for the electrode reactions. Zhu et al carried out a modeling study on the enhancement of TPB of nano-structured electrodes by infiltration [123]. The model is based on the random packing of sphere particles and electronic or ionic conducting scaffold coated with a continuous nanoparticle layer, see Fig. 12 [123]. The results predict the substantial increase in the TPB length, e.g., 6.2 and 14.6 times higher as compared to conventional mixed composites when the infiltrated nanoparticle size is 50 and 20 nm, respectively (assuming the particle size of conventional composite phase is 1 μm). The finite element calculation based on a model structure consisted of micrometer-scale columns and nano-scale branches of ionically conducting materials also shows that the increase in the surface area of the infiltrated mixed conductor could result in a factor of 10 polarization resistance decrease [124]. Based on a simple model, Shah et al predicted the apparent saturation in performance enhancement at higher infiltrate loading most likely due to the dominated ionic transport limitation at the scaffold [125].

As shown in Table 1, the promotion factor varies significantly for nano-structured cathodes and anodes, 2.3–78 for

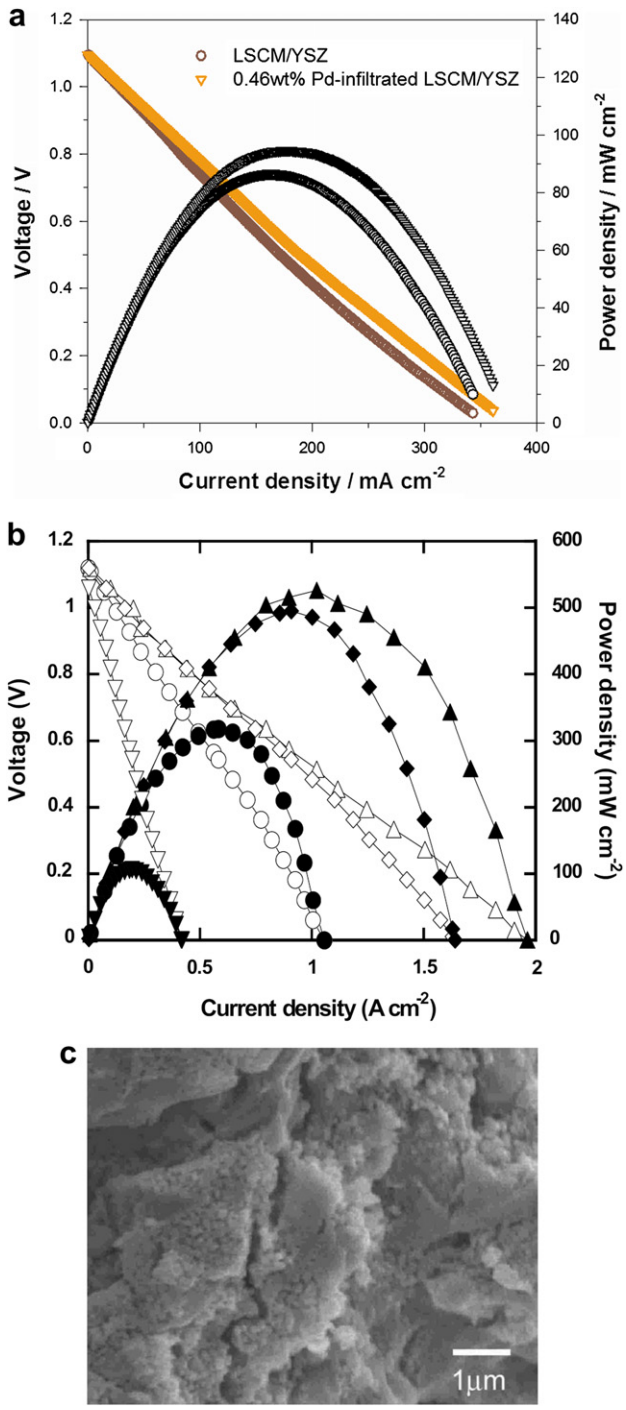

Fig. 11 – Cell performance in humidified H_2 (3% H_2O) of (a) conventional LSCM/YSZ composite anodes with and without Pd infiltration at 800 °C and the infiltrated Pd loading was ~0.46 wt% [85]; (b) infiltrated LSCM/YSZ composite anodes at 700 °C, where (∇) pure LSCM/YSZ anodes, (○) with 5 wt% ceria, (◇) with 0.5 wt% Pd, and (Δ) with 5wt% ceria and 0.5 wt% Pd; and (c) SEM micrograph of an infiltrated LSCM/YSZ composite anodes after reduced in humidified H_2 at 800 °C for 4 h [95].

the O_2 reduction reactions, 1.6–25 for the H_2 oxidation reaction and 4.6–26 for the CH_4 oxidation reaction. The wide variations of the promotion factors are clearly due to the significant differences in the microstructure, electronic and ionic properties of the scaffold, and to the distribution, loading and catalytic activities of the infiltrated nanoparticles. The observed significant promotion effect of the nano-structured electrodes with discretely distributed nanoparticles (i.e., nanoparticles are not interconnected) indicates that there must be significant catalytic effects of the infiltrated nanoparticles on the electrochemical performance of the electrodes in addition to the obviously enhanced TPB. This is particularly true that in the case of metallic nanoparticles (e.g., Pd), the amounts of metallic nanoparticles required to provide significant enhancement in electrode performance are so small that the effect must be catalytic.

Early studies on the effect of infiltrated GDC nanoparticles on the performance and electrode behavior of the LSM cathode show that the promotion effect of infiltrated GDC is far more pronounced on the electrode process at low frequencies as compared to that at high frequencies [81]. The activation energy of the electrode process at high frequencies, σ_H for O_2 reduction on the GDC-infiltrated LSM is ~100 kJ mol^{-1}, similar to that for the reaction on pure LSM [126]. On the other hand, the activation energy of the electrode process associated with low frequency arc, σ_L for the reaction on the GDC-infiltrated LSM is 140 kJ mol^{-1}, significantly lower than ~170–200 kJ mol^{-1} for the reaction on pure LSM [126]. The low activation energy of the reaction on the GDC-impregnated LSM is probably related to the low activation energy of ~74 kJ mol^{-1} for the ionic conductivity on the infiltrated GDC [127]. This indicates that the infiltration of nano-sized GDC particle phase greatly accelerates the oxygen dissociation and diffusion process in addition to the substantial reduced overall electrode polarization resistance of the nano-structured GDC-LSM cathodes for the O_2 reduction reaction. Similar promotion effect is also reported for the reaction on $Y_{0.5}Bi_{1.5}O_3$-infiltrated LSM electrodes [98].

The effect of the nano-structured electrodes on the mechanism of the O_2 reduction reaction is also studied by AFM. Fig. 13 is the AFM images of the electrode/YSZ electrolyte interface in contact with the BSCF-impregnated LSM cathodes before and after the polarization test [89]. The convex rings on the YSZ electrolyte surface are the contact interfaces between the LSM grains and YSZ electrolyte formed during the sintering of the LSM electrodes [128]. There is clearly a morphological change and broadening of the convex rings after the polarization at 200 mA cm^{-2} and 700 °C for 120 h for the reaction on the pure LSM cathode, as compared to that before the polarization (Fig. 13a and b). The morphological change of the convex rings is the direct indications of the O_2 reduction reactions that take place at the LSM/YSZ interface [128]. In contrast to that of the pure LSM cathode, the morphological changes of the convex rings on the YSZ electrolyte surface in the case of the nano-structured BSCF-infiltrated LSM cathodes before and after polarization treatment are negligible (Fig. 13c and d). This indicates that the O_2 reduction reaction is no longer restricted to the electrode/electrolyte interface region in the case of the nano-structured BSCF-LSM cathodes. Instead, the TPBs for the O_2 reduction reaction extend to the bulk of the electrode.

Among the metallic nanoparticles, infiltrated Pd nanoparticles are the most interesting and widely studied catalysts for the O_2 reduction and in particular the hydrocarbon

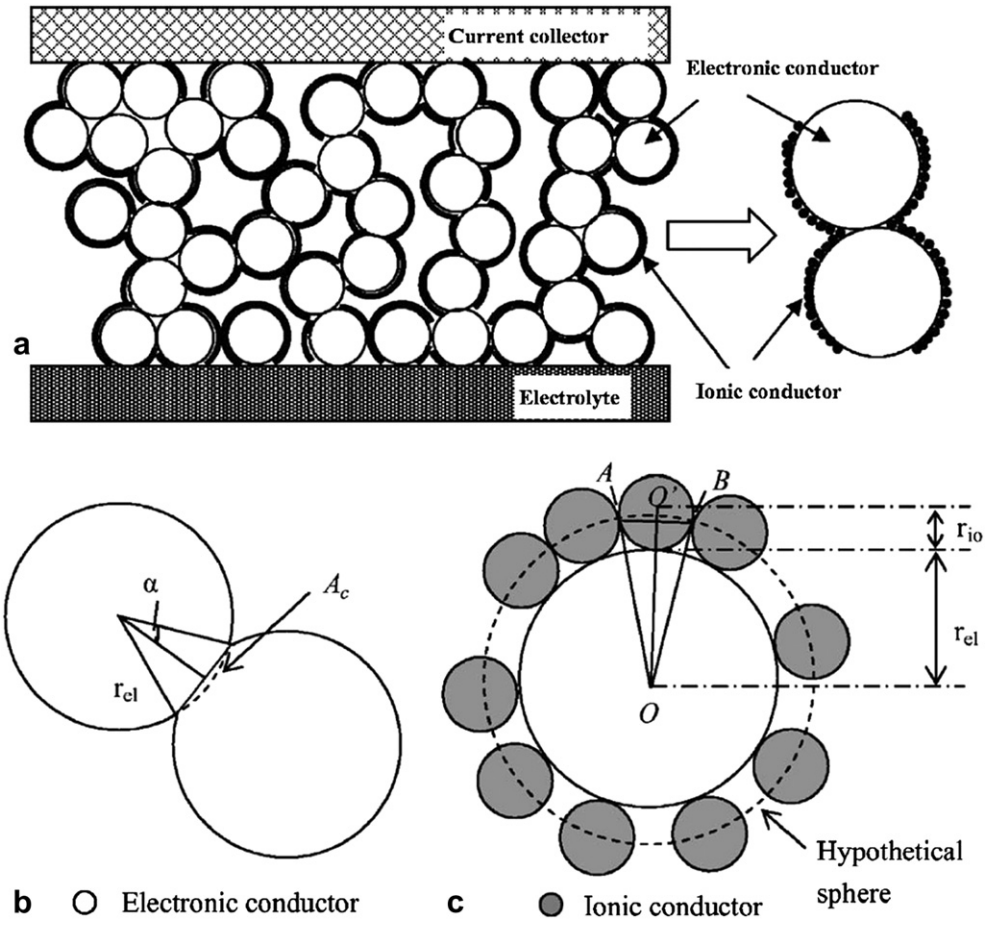

Fig. 12 – Modeling approach based on the random packing of sphere particles and electronic or ionic conducting scaffold coated with a continuous nanoparticle layer [123].

oxidation reactions. The transition between nano-sized PdO and Pd occurs at temperatures of ~800 °C [129]. Even in the reducing environment, XPS studies indicate that ~27% of the surface of the infiltrated Pd nanoparticles on Ni/GDC scaffold remains as PdO [91]. The reason could be related to the presence of nickel which could retard the reducibility of palladium, forming PdO on the surface of Pd nanoparticles. Fox et al. [130] studied the reducibility of bimetallic PdCu/CeO_2 catalysts and showed that mutual interaction between Cu, Pd and CeO_2 components affects the reduction process. The presence of copper significantly retards the reducibility of Pd on ceria at high temperatures probably due to the greater oxygen affinity of copper over palladium. The presence of Pd/PdO redox couples appears to play a critical role in the promotion of the H_2 oxidation on the Ni/GDC anodes. Fig. 14 shows the impedance curves of the H_2 oxidation reaction on Ni/GDC cermet anodes as a function of the infiltrated Pd loading in 97%H_2/3%H_2O at 850 °C. For the oxidation reaction of H_2 on the pure Ni/GDC anode, the impedance responses are characterized by a large impedance arc with no clear separation in the impedance frequency range studied. The impedance arc for the H_2 oxidation reaction on Ni/GDC anodes decreases with the infiltrated Pd nanoparticles, indicating the significant promotion effect of the Pd on the H_2 oxidation reaction. The most interesting observation is that the impedance responses of the H_2 oxidation reaction on the Pd-infiltrated Ni/GDC anodes become clearly separated at low and high frequencies. The clear separation of the electrode processes indicates that the promotion effect of infiltrated Pd nanoparticle phase is also preferential toward particular electrode processes taking place on the Ni/GDC anode.

The preferential catalytic effect of infiltrated Pd on the H_2 oxidation reaction on Ni/GDC anodes is also indicated by the dependence of the activation energies of the electrode processes associated with low and high frequency arcs, R_L and R_H on the loading of the infiltrated Pd phase, as shown in Fig. 15 [91]. The activation energy of R_L decreases almost linearly with the increasing Pd loading, while for R_H it is independent of the infiltrated Pd loading. The significant reduction in the activation energy for the hydrogen dissociation and diffusion process (i.e., the process associated with the low frequencies, R_L) is most likely due to the accelerated hydrogen and oxygen spillover mechanism over the Pd/PdO redox couple on the Ni/GDC anodes. The observed significant promoting effect of infiltrated Pd nanoparticles on the oxidation reaction of methane and ethanol (see Fig. 7c and d) is most likely related to the high catalytic activity of palladium on the dissociation and activation of methane and ethanol and subsequent gasification and oxidation of carbon and hydrogen species [131]. However, it should be pointed out here

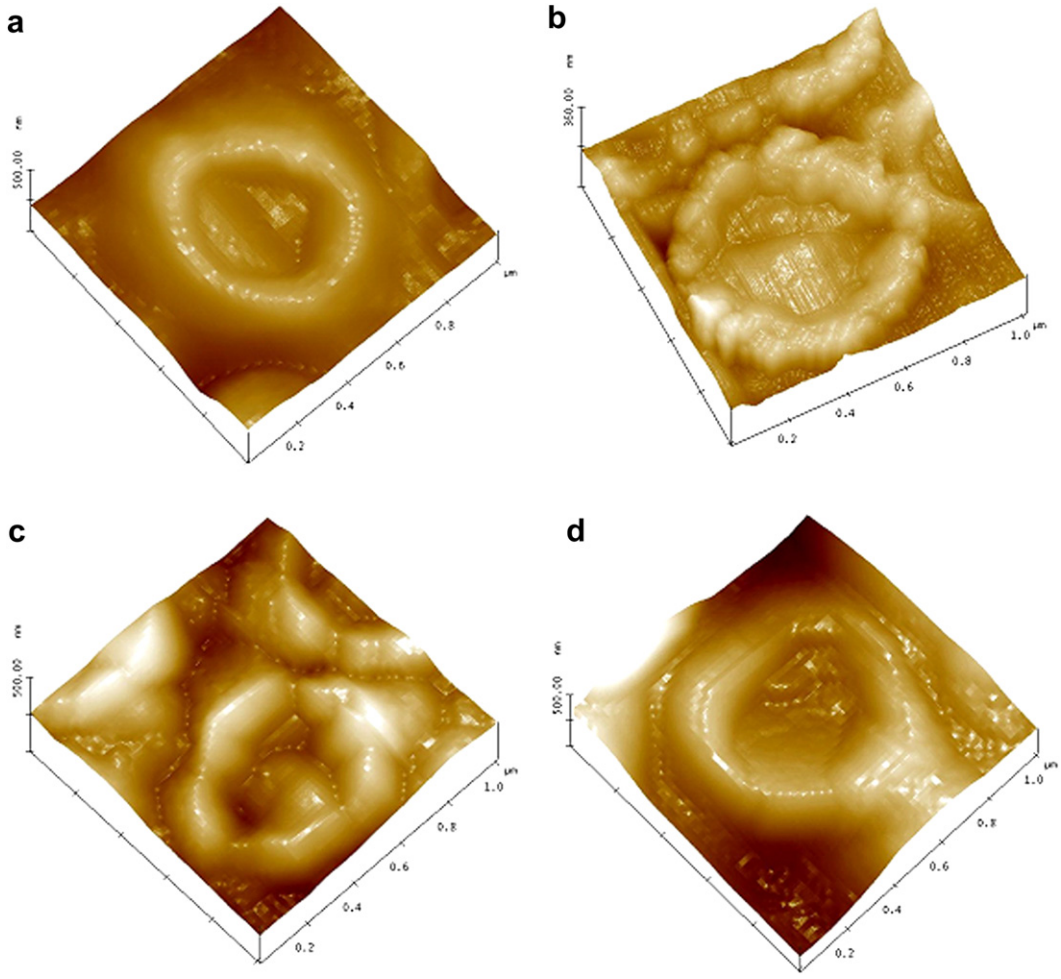

Fig. 13 – AFM micrographs of the YSZ surface in contact with the cathodes: (a) before and (b) after cathodic current passage at 200 mA cm^{-2}, 700 °C for 120 h for the pure LSM cathode and (c) before and (d) after cathodic current passage at 200 mA cm^{-2}, 700 °C for 120 h for the 1.2 mg cm^{-2} BSCF-infiltrated LSM cathode. Electrode coatings were removed by HCl treatment [89].

that unique catalytic activity of infiltrated nanoparticles is not limited to Pd. Other metals such as infiltrated Rh, Ni and Fe also show high catalytic activity for the anode reactions in SOFCs [95].

Most interesting, infiltrated Pd nanoparticles are very effective for the promotion of the O_2 reduction reactions. Fig. 16 is the impedance responses of the conventional LSM/YSZ, LSM infiltrated YSZ (LSM + YSZ) and Pd-infiltrated LSM/YSZ (Pd + LSM-YSZ) composite cathodes measured at 700 °C in air at open circuit [92]. The electrode polarization resistance of nano-structured LSM + YSZ cathode is substantially smaller than that on the conventional LSM/YSZ composite cathodes, clearly due to the substantially increased TPB as the results of the nanoscale engineering of the conventional LSM/YSZ composite (e.g., see Fig. 9). The R_E value of the Pd + LSM/YSZ cathode is 0.18 Ωcm^2 at 700 °C, which is comparable to those of the MIEC cathodes like LSCF (0.32 Ωcm^2 at 700 °C [11]) and $Gd_{0.8}Sr_{0.2}CoO_3$ (0.10 Ωcm^2 at 700 °C [132]). The activation energy of the O_2 reduction reaction on nano-structured Pd + LSM/YSZ composite cathodes is 96 kJ mol^{-1}, also significantly lower than 163 kJ mol^{-1} on conventional LSM/YSZ composite cathodes [92]. This indicates that nano-structure reduces the energy barrier for the O_2 reduction reaction as compared to that on micro-structured conventional electrodes. The observed inductance loop for the O_2 reduction reaction appears to be closely associated with the nano-structured electrodes [56,87,90,92]. Pd was also shown to significantly increase the electrochemical activity of SSC/$La_{0.8}Sr_{0.2}Mg_{0.15}Co_{0.05}O_3$ composite cathodes [133]. Pd may incorporate into perovskite structure such as LSCF, adjusting the surface composition and thus enhancing the catalytic activity of the electrode, as proposed by Serra and Buchkremer [134].

However, there are significant discrepancies of the electrocatalytic roles of the infiltrated nanoaprticles. Bidrawn et al studied the effect of the microstructure of the host scaffolds of infiltrated LSM/YSZ and LSF/YSZ electrodes on the infiltrated nanoparticles [135]. The addition of CeO_2, SDC, Pd, YSZ, CaO and K_2O had little effect on the infiltrated LSF/YSZ and LSM/YSZ pre-sintered at 850 °C but showed more or less similar improvement to the electrodes pre-sintered at a much higher temperature of 1100 °C. They claim that the enhancement

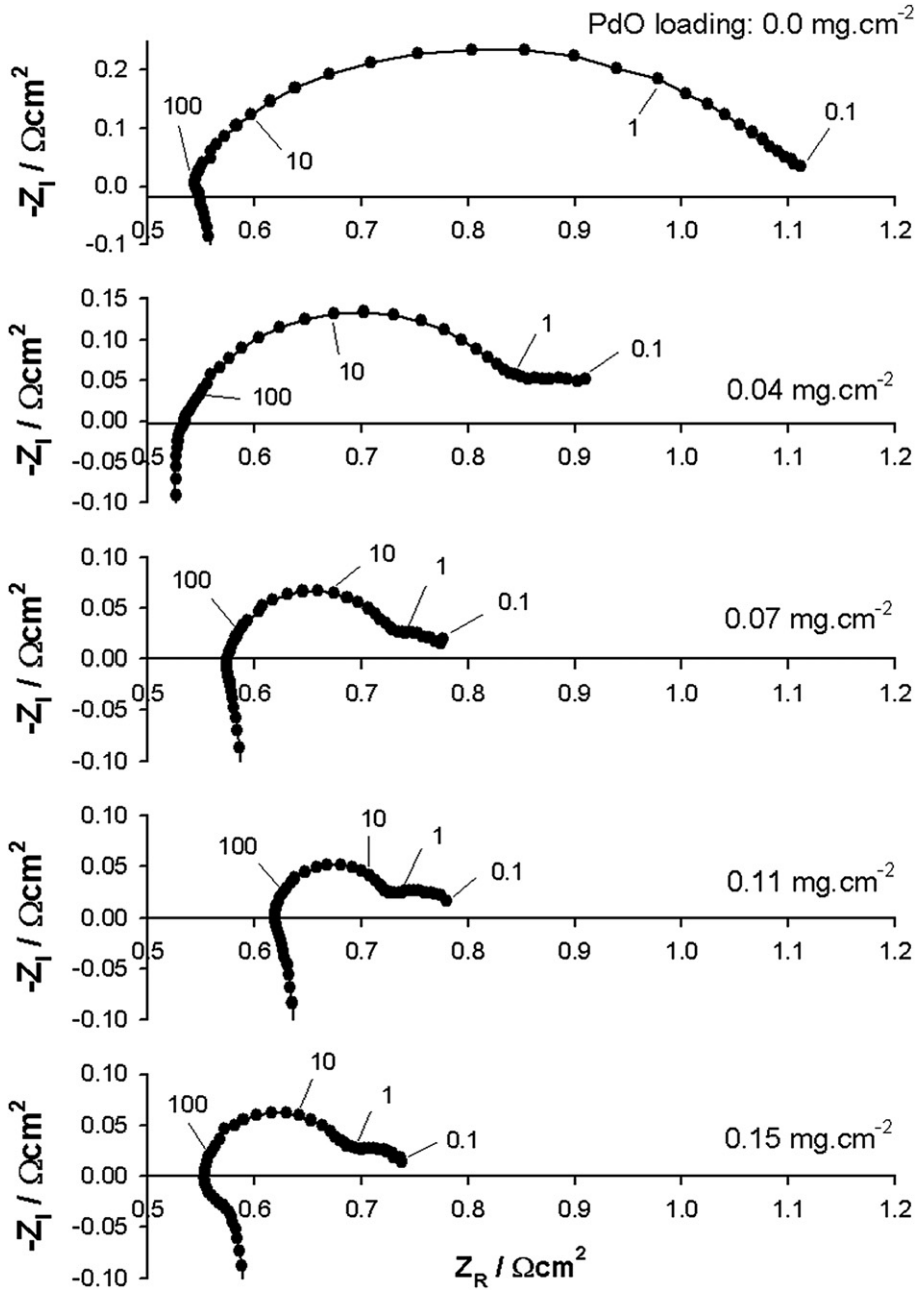

Fig. 14 – Impedance spectra for the H_2 oxidation reaction on Pd-infiltrated Ni/GDC cermet anode as a function of PdO loading in 97%H_2/3%H_2O at 850 °C. Numbers are frequencies in Hz [91].

associated with addition of a catalyst is simply an artifact of structure [135]. Yamahara et al reported a significant decrease in the electrode polarization resistance of cobalt-infiltrated LSM cathodes [136], while Huang et al showed that addition of 10 wt % CoO_x to an LSM/YSZ composite has basically no effect on the cathode performance [137]. A study by Imanishi et al showed that addition of cobalt oxide by infiltration significantly reduced the polarization overpotentials of the LSM/YSZ composite cathodes at temperatures 600–800 °C [138]. An early study by Haanappel et al showed that LSM cathodes are indistinguishable with or without addition of Pd [139]. On the other hand, work carried out in our laboratory consistently showed that infiltrated Pd has remarkable promoting effect on the LSM, LSM/YSZ, and LSCF electrodes for the O_2 reduction reaction [90,117].

Though the enhancement of the addition of inert materials such as CaO and K_2O on the performance of LSF/YSZ scaffold as observed by Bidrawn et al. [135] is difficult to comprehend, a study by Hansen et al. [140] showed that infiltration of LSM in general improves the performance of LSM/YSZ cathodes, and adding inert alumina nano-particles had a detrimental effect on the activity of the LSM/YSZ composite electrodes. Lee et al studied the effect of ionic conductive LSC and electrically insulating Sr-doped $La_2Zr_2O_7$ (LSZ) infiltrated SDC/

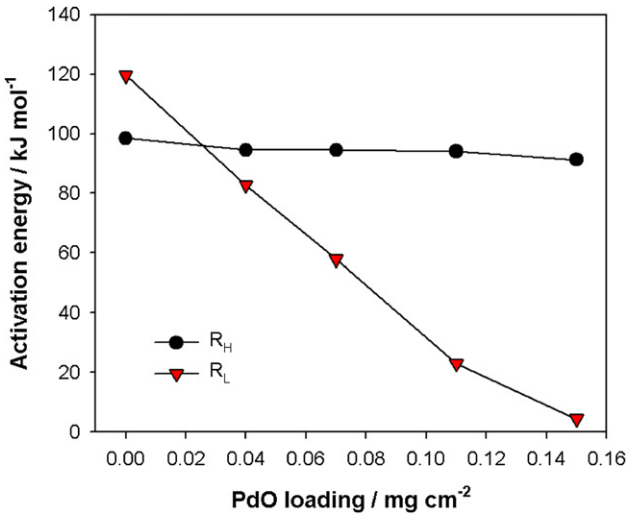

Fig. 15 – Plot of the activation energies of high frequency arc resistance (R_H) and low frequency arc resistance (R_L) as a function of the infiltrated PdO loading for the hydrogen oxidation reaction on Pd-infiltrated Ni/GDC cermet anodes [91].

LSCF cathodes [141]. The LSC-infiltrated SDC/LSCF cathodes improved the performance, while infiltration of LSZ has a negative effect on the performance. The detrimental effect of the infiltrated LSZ increased with the increased infiltrated loading of the insulated LSZ phase. A well-designed study of the LSCF model electrode infiltrated with a thin layer of LSM demonstrated that efficient electrode architecture is critical for the catalytic role of the infiltrated nanoparticles or films, see Fig. 17 [142]. The ASR of the LSM-coated LSCF cathode is larger at OCV but smaller under the cathodic bias. In contrast with the continuous degradation of the cell with LSCF model cathodes, the cell with LSM-infiltrated LSCF cathodes show a time-dependent activation phenomena. The results show that the infiltrated LSM film plays an important catalytic role

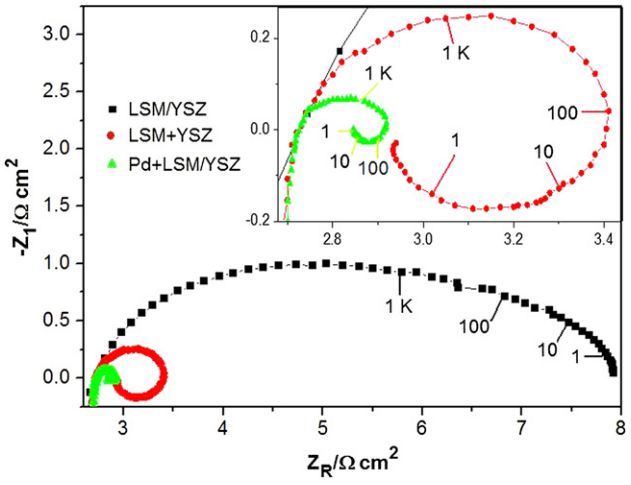

Fig. 16 – Electrochemical impedance spectra of the conventional LSM/YSZ, nano-structured LSM + YSZ and Pd + LSM/YSZ composite cathodes measured at 700 °C in air at open circuit. Numbers are frequencies in Hz [92].

in the promotion of the surface oxygen adsorption and/or dissociation and in the polarization-induced activation process. DFT calculation showed that adsorption energy is lower on LSM than that on LSC and LSF [143]. Evidently, such catalytic role of the infiltrated LSM nanopartilces would only be effective for the thin infiltrated LSM layer. Infiltrated Ag nanoparticle also showed the enhancement on the electrochemical activity of LSCF cathodes [94,144], most likely due to the promotion of silver for the oxygen adsorption, dissociation and diffusion. Hojberg and Sogaard showed that the activation energy for the O_2 reduction on LSM/YSZ composite cathode was decreased from 1.35 eV to 1.19 eV on the LSM/YSZ composite cathodes infiltrated with LSM and SDC [145].

5. Prospect and challenges

Nanoscale engineering approach via low temperature infiltration process has attracted increasingly attention as the most effective and alternative techniques in the development of the nano-structured electrodes to achieve high performance and advantageous microstructure in a way that otherwise would not be possible with high temperature processes for standard SOFCs electrodes. The unique advantages and flexibilities of the nanoscale engineering of the conventional electrode structure via a two-step firing approach have been clearly demonstrated on the wide range nano-structured electrodes systems for SOFCs, SOECs, metal-supported SOFCs and single-chamber SOFCs. Recent results also show that infiltration process can be used for large and practical planar cells with active areas of 81 cm^2 (100 × 100 mm cells) [146]. The results so far clearly demonstrate that infiltrated metal and metal oxide nanoparticles not only substantially increase the TPBs for the reaction but also play very important catalytic roles in the enhancement of the fuel cell reactions. The catalytic role of infiltrated nanoparticles/films depends on both morphology and microstructure of the infiltrated phase and the nature of the scaffold supports.

One of the most challenging problems associated with a SOFC system over a 3–5 year lifetime is the gradual degradation and deactivation of the cathodes and anodes by contaminants which can be either in the air or fuel streams or from the volatile species of cell components, such as metallic interconnect, sealant and manifold [147]. Thus in practical SOFC systems, the electrodes not only need to be high performance but also need to be very stable and tolerant toward various contaminants including chromium, boron, sulfur, carbon, silica, etc [147]. Nano-structured electrodes already show specific tolerance toward the carbon deposition [83,84] and poisoning of sulfur [148] and chromium [149]. Nano-structured electrodes based on infiltration are not limited to one electrocatalytic active species and in principle, it is possible to develop nano-structured electrodes with high activity and tolerance toward contaminants with infiltration of multiple nanoparticles phases with specific functions and activities.

Consequently, the most significant challenge in the application and development of nano-structured electrodes is the long-term stability of the microstructure and activity of the infiltrated nanoparticles. As the particle size of the infiltrated phase is very fine (20–100 nm), the tendency for sintering and

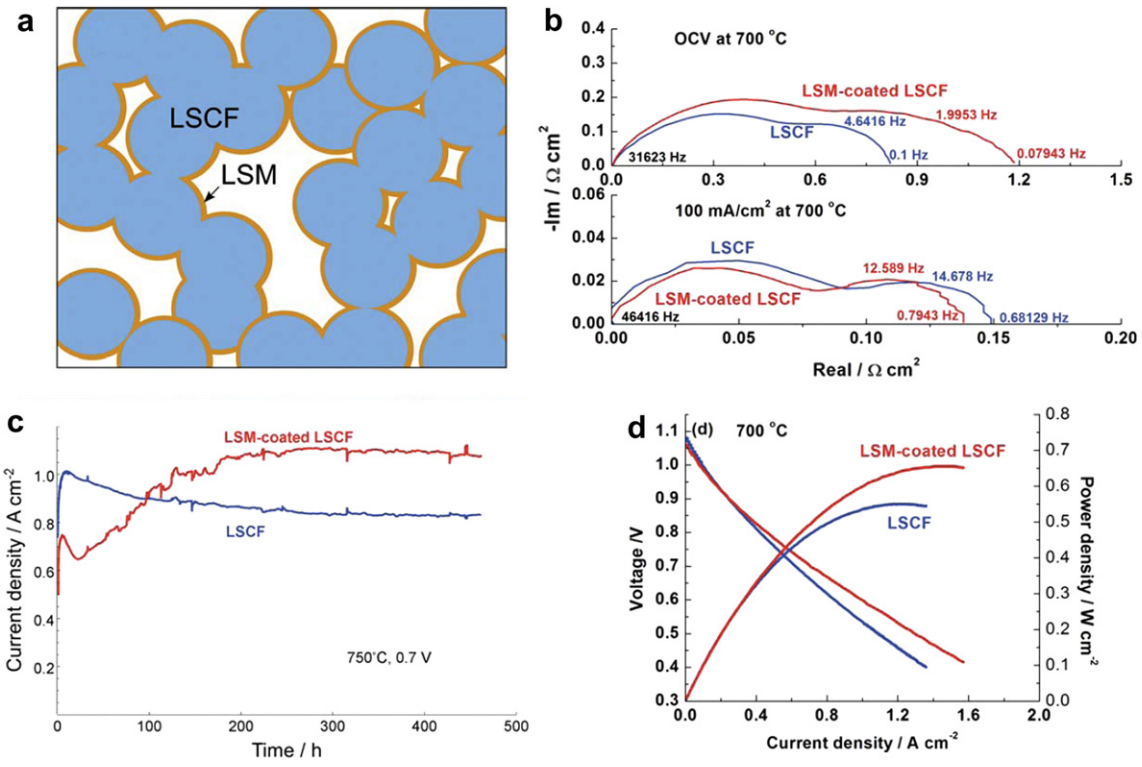

Fig. 17 – (a) Schematic diagram of the LSM-infiltrated LSCF cathode. (b) Impedance spectra of fuel cells with and without infiltration of LSM measured at OCV and at 100 mA cm^{-2}, without Ohmic portion. (c) Current density of two test cells with and without infiltration as a function of time under a constant voltage of 0.7 V and approximate cathodic overpotential of −0.12 V. (d) Cell voltages and power densities as a function of current density for full cells with and without infiltration of LSM after long-term testing [142].

grain growth at operation temperature of SOFCs (500–800 °C) would be high due to the large surface energy associated with the nano-sized oxide or metallic phase [150]. Wang et al studied the stability of LSF infiltrated YSZ composite cathodes at 700 °C and the ASR increased linearly with time for the infiltrated composite cathodes calcined at 850 °C [151]. In the case of infiltrated Pd nanoparticles on porous YSZ scaffold, the agglomeration and grain growth would result in the formation of continuous and dense Pd films on the YSZ scaffold surface, leading to the increase in the polarization losses due to the blocking of the oxygen diffusion path [152]. Alloying with cobalt, manganese and silver has been found to be effective to increase the thermal stability and to enhance the performance stability of Pd-infiltrated electrodes [152,153]. Kim et al showed recently that highly active and stable Pd catalysts can be obtained by infiltrate Pd@CeO_2 core-shell nanoparticles into YSZ scaffold [119]. The core-shell nanostructure inhibits the growth of Pd nanoparticles. Co-infiltration of mixed ceria and cobalt solutions was also found to suppress the aggregation of Co_3O_4 nanoparticles [138]. Zhao et al showed that excellent thermal cycle durability can be achieved by the nano-structured LSC-$Sm_{0.2}Ce_{0.8}O_2$ cathodes, see Fig. 18 [93,154]. The high stability of the infiltrated LSC-SDC cathodes is most likely due to the formation of a continuous and stable LSC nanoparticles anchored on the SDC scaffold. The modeling study suggests that the size of the nanoparticles is probably the most important factor to stabilize the nanostructure during the thermal cycle [155]. Nevertheless, the long-term stability of nano-structured electrodes on large and practical cells has not been demonstrated yet. Multiple component infiltration, selective alloying or nano-structured engineering such as core-shell catalysts may provide solutions to enhance the structural stability of the infiltrated nano-structures [119,152]. On the other hand, Ni infiltrated

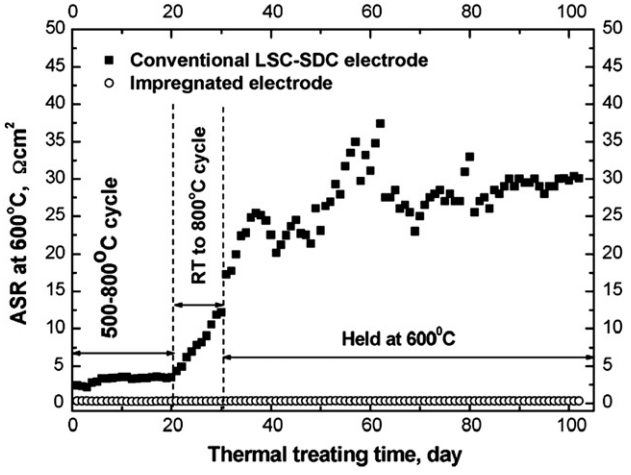

Fig. 18 – ASR at 600 °C for the infiltrated LSC-SDC cathode and conventional LSC-SDC cathodes as a function of thermal treatment [154].

YSZ composite anodes showed no dimensional changes after one redox cycle, indicating the potential as the redox stable Ni-based anodes of SOFCs [156].

Discrepancies for the promotion effect of infiltrated nanoparticles on the performance and electrode reactions of SOFCs are a significant issue in the development and understanding of the nanoscale and nano-structured electrodes based on infiltration. Part of the discrepancies could be related to differences in the infiltration process such as heat-treatment temperature, surfactant in the infiltration solutions, and the loading and distribution of the infiltrated phase. Another reason could be due to the fact that the catalytic effect of the infiltrated phases depends strongly on the architect or the morphology and microstructure of the infiltrated nanoparticles or films as demonstrated by Liu et al. [142], the nature of the porous scaffold, as observed for the significant different effects of infiltrated Pd on Ni/GDC and LSCM scaffolds [85,88,91,95], and the potential interaction between the scaffold and infiltrated phase [134]. The activation and deactivation phenomena of SOFC cathodes, which depends strongly on the microstructure, polarization and presence of other phases [157–159] and the phase segregation at the electrode/electrolyte interface [160,161] also complicate the mechanism of the promotion effect of infiltrated nanoparticles.

Despite the multiple step nature associated with the infiltration method, nanoscale engineering of electrode structures via infiltration is probably the most effective way to develop highly active and advanced electrode structures for SOFCs. However, much more systematic and extensive studies and long-term tests are needed to fundamentally understand the promotion mechanism of the infiltrated nanoparticles and to fully assess the structural and performance stability of the nanoscale engineered electrodes under SOFCs operation conditions. The modeling simulations can be very useful and important in the fundamental and structural stability assessment of nano-structured electrodes [64,123–125,155,162], particularly if the microstructural as well as electrochemical and catalytic aspects of the infiltrated nanoparticle are incorporated into the models.

Acknowledgment

I would like to knowledge the support by the Curtin Fellowship start-up fund and ARC Linkage Project (LP110200281), Australia.

REFERENCES

[1] Chen AC, Holt-Hindle P. Platinum-based nanostructured materials: synthesis, properties, and applications. Chem Rev 2010;110:3767–804.
[2] Badwal SPS. Zirconia-based solid electrolytes - microstructure, stability and ionic-conductivity. Solid State Ionics 1992;52:23–32.
[3] Kharton VV, Marques FMB, Atkinson A. Transport properties of solid oxide electrolyte ceramics: a brief review. Solid State Ionics 2004;174:135–49.
[4] Ishihara T. Development of new fast oxide ion conductor and application for intermediate temperature solid oxide fuel cells. Bull Chem Soc Jpn 2006;79:1155–66.
[5] Brett DJL, Atkinson A, Brandon NP, Skinner SJ. Intermediate temperature solid oxide fuel cells. Chem Soc Rev 2008;37:1568–78.
[6] Jiang SP. A review of wet impregnation – An alternative method for the fabrication of high performance and nano-structured electrodes of solid oxide fuel cells. Mater Sci Eng A-Struct Mater Prop Microstruct Process 2006;418:199–210.
[7] Jiang SP. Issues on development of (La, Sr)MnO_3 cathode for solid oxide fuel cells. J Power Sources 2003;124:390–402.
[8] Jiang SP. Development of lanthanum strontium manganite perovskite cathode materials of solid oxide fuel cells: a review. J Mater Sci 2008;43:6799–833.
[9] Sakaki Y, Takeda Y, Kato A, Imanishi N, Yamamoto O, Hattori M, et al. Ln1-xSrxMnO_3 (Ln = Pr, Nd, Sm and Gd) as the cathode material for solid oxide fuel cells. Solid State Ionics 1999;118:187–94.
[10] Carter S, Selcuk A, Chater RJ, Kajda J, Kilner JA, Steele BCH. Oxygen-transport in selected nonstoichiometric perovskite-structure oxides. Solid State Ionics 1992;53-6:597–605.
[11] Jiang SP. A comparison of O_2 reduction reactions on porous (La, Sr)MnO_3 and (La, Sr)(Co, Fe)O_3 electrodes. Solid State Ionics 2002;146:1–22.
[12] Murray EP, Tsai T, Barnett SA. Oxygen transfer processes in (La, Sr)MnO_3/Y_2O_3-stabilized ZrO_2 cathodes: an impedance spectroscopy study. Solid State Ionics 1998;110:235–43.
[13] Murray EP, Barnett SA. (La, Sr) MnO_3-(Ce, Gd)O_2-x composite cathodes for solid oxide fuel cells. Solid State Ionics 2001;143:265–73.
[14] Esquirol A, Brandon NP, Kilner JA, Mogensen M. Electrochemical characterization of $La_{0.6}Sr_{0.4}Co_{0.2}Fe_{0.8}O_3$ cathodes for intermediate-temperature SOFCs. J Electrochem Soc 2004;151:A1847–55.
[15] Ding C, Hashida T. High performance anode-supported solid oxide fuel cell based on thin-film electrolyte and nanostructured cathode. Energy Environ Sci 2010;3:1729–31.
[16] Usui T, Ito Y, Kikuta K. Fabrication and characterization of LSCF-GDC/GDC/NiO-GDC microtubular SOFCs prepared by multi-dip coating. J Ceram Soc Jpn 2010;118:564–7.
[17] Hwang HJ, Ji-Woong MB, Seunghun LA, Lee EA. Electrochemical performance of LSCF-based composite cathodes for intermediate temperature SOFCs. J Power Sources 2005;145:243–8.
[18] Park YM, Kim JH, Kim H. High-performance composite cathodes for solid oxide fuel cells. Int J Hydrog Energy 2011;36:9169–79.
[19] Shao ZP, Haile SM. A high-performance cathode for the next generation of solid-oxide fuel cells. Nature 2004;431:170–3.
[20] Wei B, Lu Z, Li SY, Liu YQ, Liu KY, Su WH. Thermal and electrical properties of new cathode material $Ba_{0.5}Sr_{0.5}Co_{0.8}Fe_{0.2}O_3$-delta for solid oxide fuel cells. Electrochem Solid State Lett 2005;8:A428–31.
[21] Jiang SP, Love JG, Apateanu L. Effect of contact between electrode and current collector on the performance of solid oxide fuel cells. Solid State Ionics 2003;160:15–26.
[22] Yan AY, Yang M, Hou ZF, Dong YL, Cheng MJ. Investigation of Ba1-xSrx$Co_{0.8}Fe_{0.2}O_3$-delta as cathodes for low-temperature solid oxide fuel cells both in the absence and presence of CO_2. J Power Sources 2008;185:76–84.
[23] Laberty C, Zhao F, Swider-Lyons KE, Virkar AV. High-performance solid oxide fuel cell cathodes with lanthanum-nickelate-based composites. Electrochem Solid State Lett 2007;10:B170–4.
[24] Chiba R, Yoshimura F, Sakurai Y. An investigation of LaNi1-x$FexO_3$ as a cathode material for solid oxide fuel cells. Solid State Ionics 1999;124:281–8.

[25] Bastidas DM, Tao SW, Irvine JTS. A symmetrical solid oxide fuel cell demonstrating redox stable perovskite electrodes. J Mater Chem 2006;16:1603–5.
[26] Tarancon A, Skinner SJ, Chater RJ, Hernandez-Ramirez F, Kilner JA. Layered perovskites as promising cathodes for intermediate temperature solid oxide fuel cells. J Mater Chem 2007;17:3175–81.
[27] Yokokawa H. Understanding materials compatibility. Ann Rev Mater Res 2003;33:581–610.
[28] Simner SP, Bonnett JF, Canfield NL, Meinhardt KD, Sprenkle VL, Stevenson JW. Optimized lanthanum ferrite-based cathodes for anode-supported SOFCs. Electrochem Solid State Lett 2002;5:A173–5.
[29] Simner SP, Bonnett JR, Canfield NL, Meinhardt KD, Shelton JP, Sprenkle VL, et al. Development of lanthanum ferrite SOFC cathodes. J Power Sources 2003;113:1–10.
[30] Martinez-Amesti A, Larranaga A, Rodriguez-Martinez LM, Aguayo AT, Pizarro JL, No ML, et al. Reactivity between La(Sr)FeO_3 cathode, doped CeO_2 interlayer and yttria-stabilized zirconia electrolyte for solid oxide fuel cell applications. J Power Sources 2008;185:401–10.
[31] Anderson MD, Stevenson JW, Simner SP. Reactivity of lanthanide ferrite SOFC cathodes with YSZ electrolyte. J Power Sources 2004;129:188–92.
[32] Tu HY, Takeda Y, Imanishi N, Yamamoto O. Ln(0.4)Sr(0.6) Co(0.8)Fe(0.2)O(3-delta) (Ln = La, Pr, Nd, Sm, Gd) for the electrode in solid oxide fuel cells. Solid State Ionics 1999; 117:277–81.
[33] Peters C, Weber A, Ivers-Tiffee E. Nanoscaled ($La_{0.5}Sr_{0.5}$) CoO_3-delta thin film cathodes for SOFC application at 500 °C < T < 700 °C. J Electrochem Soc 2008;155:B730–7.
[34] Jiang SP, Chan SH. A review of anode materials development in solid oxide fuel cells. J Mater Sci 2004;39: 4405–39.
[35] Jiang SP. A comparative study of fabrication and performance of Ni/3 mol % Y_2O_3-ZrO_2 and Ni/8 mol% Y_2O_3-ZrO_2 cermet electrodes. J Electrochem Soc 2003;150: E548–59.
[36] Zha SW, Cheng Z, Liu ML. Sulfur poisoning and regeneration of Ni-based anodes in solid oxide fuel cells. J Electrochem Soc 2007;154:B201–6.
[37] Eguchi K, Kojo H, Takeguchi T, Kikuchi R, Sasaki K. Fuel flexibility in power generation by solid oxide fuel cells. Solid State Ion 2002;152–153:411–6.
[38] Zha S, Tsang P, Cheng Z, Liu M. Electrical properties and sulfur tolerance of La0.75Sr0.25Cr1-xMnxO3 under anodic conditions. J Solid State Chem 2005;178:1844–50.
[39] Mukundan R, Brosha EL, Garzon FH. Sulfur tolerant anodes for SOFCs. Electrochemical Solid-State Lett 2004;7:A5–7.
[40] Aguilar L, Zha S, Li S, Winnick J, Liu M. Sulfur-Tolerant materials for the hydrogen sulfide SOFC. Electrochemical Solid-State Lett 2004;7:A324–6.
[41] Marina OA, Pederson LR. Novel ceramic anodes for SOFCs tolerant to oxygen, carbon and sulfur. In: Huijismans J, editor. The fifth European solid oxide fuel cell forum. Lucerne, Switzerland: European Fuel Cell Forum; 2002. p. 481–9.
[42] Marina OA, Canfield NL, Stevenson JW. Thermal, electrical, and electrocatalytical properties of lanthanum-doped strontium titanate. Solid State Ionics 2002;149:21–8.
[43] Tao S, Irvine JTS. Optimization of mixed conducting properties of Y_2O_3-ZrO_2-TiO_2 and Sc_2O_3-Y_2O_3-ZrO_2-TiO_2 solid solutions as potential SOFC anode materials. J Solid State Chem 2002;165:12–8.
[44] Slater PR, Fagg DP, Irvine JTS. Synthesis and electrical characterisation of doped perovskite titanates as potential anode materials for solid oxide fuel cells. J Mater Chem 1997;7:2495–8.
[45] Slater PR, Irvine JTS. Niobium based tetragonal tungsten bronzes as potential anodes for solid oxide fuel cells: synthesis and electrical characterisation. Solid State Ionics 1999;120:125–34.
[46] Tao SW, Irvine JTS. A redox-stable efficient anode for solid-oxide fuel cells. Nat Mater 2003;2:320–3.
[47] Huang YH, Dass RI, Xing ZL, Goodenough JB. Double perovskites as anode materials for solid-oxide fuel cells. Science 2006;312:254–7.
[48] Jiang SP, Liu L, Ong KP, Wu P, Li J, Pu J. Electrical conductivity and performance of doped $LaCrO_3$ perovskite oxides for solid oxide fuel cells. J Power Sources 2008;176: 82–9.
[49] Gorte RJ, Vohs JM. Nanostructured anodes for solid oxide fuel cells. Curr Opin Colloid Interface Sci 2009;14:236–44.
[50] Vohs JM, Gorte RJ. High-performance SOFC cathodes prepared by infiltration. Adv Mater 2009;21:943–56.
[51] Jiang ZY, Xia CR, Chen FL. Nano-structured composite cathodes for intermediate-temperature solid oxide fuel cells via an infiltration/impregnation technique. Electrochim Acta 2010;55:3595–605.
[52] Sholklapper TZ, Jacobson CP, Visco SJ, De Jonghe LC. Synthesis of dispersed and contiguous nanoparticles in solid oxide fuel cell electrodes. Fuel Cells 2008;8:303–12.
[53] Mitterdorfer A, Gauckler LJ. $La_2Zr_2O_7$ formation and oxygen reduction kinetics of the $La_{0.85}Sr_{0.15}MnyO_3$, O-2(g)vertical bar YSZ system. Solid State Ionics 1998;111:185–218.
[54] Jiang SP, Callus PJ, Badwal SPS. Fabrication and performance of Ni/3 mol% Y_2O_3-ZrO_2 cermet anodes for solid oxide fuel cells. Solid State Ionics 2000;132:1–14.
[55] Jiang SP, Duan YY, Love JG. Fabrication of high-performance $NiOY_2O_3$-ZrO_2 cermet anodes of solid oxide fuel cells by ion impregnation. J Electrochem Soc 2002;149:A1175–83.
[56] Liang FL, Chen J, Cheng JL, Jiang SP, He TM, Pu J, et al. Novel nano-structured Pd plus yttrium doped ZrO_2 cathodes for intermediate temperature solid oxide fuel cells. Electrochem Commun 2008;10:42–6.
[57] Huang YY, Vohs JM, Gorte RJ. Fabrication of Sr-doped LaFeO(3)YSZ composite cathodes. J Electrochem Soc 2004; 151:A646–51.
[58] Sholklapper TZ, Lu C, Jacobson CP, Visco SJ, De Jonghe LC. LSM-infiltrated solid oxide fuel cell cathodes. Electrochem Solid State Lett 2006;9:A376–8.
[59] Sholklapper TZ, Kurokawa H, Jacobson CP, Visco SJ, De Jonghe LC. Nanostructured solid oxide fuel cell electrodes. Nano Lett 2007;7:2136–41.
[60] Lu C, Sholklapper TZ, Jacobson CP, Visco SJ, De Jonghe LC. LSM-YSZ cathodes with reaction-infiltrated nanoparticles. J Electrochem Soc 2006;153:A1115–9.
[61] Jiang ZY, Xia CR, Zhao F, Chen FL. $La_{0.85}Sr_{0.15}MnO_3$-delta infiltrated $Y_{0.5}Bi_{1.5}O_3$ cathodes for intermediate-temperature solid oxide fuel cells. Electrochem Solid State Lett 2009;12:B91–3.
[62] Jiang ZY, Lei ZW, Ding B, Xia CR, Zhao F, Chen FL. Electrochemical characteristics of solid oxide fuel cell cathodes prepared by infiltrating (La, Sr)MnO_3 nanoparticles into yttria-stabilized bismuth oxide backbones. Int J Hydrog Energy 2010;35:8322–30.
[63] Li W, Lue Z, Zhu X, Guan B, Wei B, Guan C, et al. Effect of adding urea on performance of Cu/CeO(2)/yttria-stabilized zirconia anodes for solid oxide fuel cells prepared by impregnation method. Electrochim Acta 2011;56:2230–6.
[64] Nicholas JD, Barnett SA. Measurements and modeling of $Sm_{0.5}Sr_{0.5}CoO_3$-x-$Ce_{0.9}Gd_{0.1}O_{1.95}$ SOFC cathodes produced using infiltrate solution additives. J Electrochem Soc 2010; 157:B536–41.
[65] Jung SW, Vohs JM, Gorte RJ. Preparation of SOFC anodes by electrodeposition. J Electrochem Soc 2007;154:B1270–5.

[66] Ai N, Jiang SP, Chen KF, Lu Z, Su WH. Vacuum-assisted electroless copper plating on Ni/(Sm, Ce)O_2 anodes for intermediate temperature solid oxide fuel cells. Int J Hydrog Energy 2011;36:7661–9.
[67] Lou XY, Liu Z, Wang SZ, Xiu YH, Wong CP, Liu ML. Controlling the morphology and uniformity of a catalyst-infiltrated cathode for solid oxide fuel cells by tuning wetting property. J Power Sources 2010;195:419–24.
[68] Park S, Craciun R, Vohs JM, Gorte RJ. Direct oxidation of hydrocarbons in a solid oxide fuel cell I. Methane oxidation. J Electrochem Soc 1999;146:3603–5.
[69] Craciun R, Park S, Gorte RJ, Vohs JM, Wang C, Worrell WL. A novel method for preparing anode cermets for solid oxide fuel cells. J Electrochem Soc 1999;146:4019–22.
[70] Park S, Gorte RJ, Vohs JM. Tape cast solid oxide fuel cells for the direct oxidation of hydrocarbons. J Electrochem Soc 2001;148:A443–7.
[71] Lee SI, Ahn K, Vohs JM, Gorte RJ. Cu–Co bimetallic anodes for direct utilization of methane in SOFCs. Electrochem Solid State Lett 2005;8:A48–51.
[72] Gorte RJ, Park S, Vohs JM, Wang CH. Anodes for direct oxidation of dry hydrocarbons in a solid-oxide fuel cell. Adv Mater 2000;12:1465–9.
[73] Park SD, Vohs JM, Gorte RJ. Direct oxidation of hydrocarbons in a solid-oxide fuel cell. Nature 2000;404:265–7.
[74] McIntosh S, Vohs JM, Gorte RJ. An examination of lanthanide additives on the performance of Cu-YSZ cermet anodes. Electrochim Acta 2002;47:3815–21.
[75] McIntosh S, Vohs JM, Gorte RJ. Effect of precious-metal dopants on SOFC anodes for direct utilization of hydrocarbons. Electrochem Solid State Lett 2003;6:A240–3.
[76] Kim G, Corre G, Irvine JTS, Vohs JM, Gorte RJ. Engineering composite oxide SOFC anodes for efficient oxidation of methane. Electrochem Solid State Lett 2008;11:B16–9.
[77] Jung SW, Lu C, He HP, Ahn KY, Gorte RJ, Vohs JM. Influence of composition and Cu impregnation method on the performance of Cu/CeO_2/YSZ SOFC anodes. J Power Sources 2006;154:42–50.
[78] Lee S, Kim G, Vohs JM, Gorte RJ. SOFC anodes based on infiltration of $La_{0.3}Sr_{0.7}TiO_3$. J Electrochem Soc 2008;155: B1179–83.
[79] McIntosh S, Gorte RJ. Direct hydrocarbon solid oxide fuel cells. Chem Rev 2004;104:4845–65.
[80] Cantos-Gomez A, Ruiz-Bustos R, van Duijn J. Ag as an alternative for Ni in direct hydrocarbon SOFC anodes. Fuel Cells 2011;11:140–3.
[81] Jiang SP, Wang W. Fabrication and performance of GDC-impregnated (La, Sr)MnO_3 cathodes for intermediate temperature solid oxide fuel cells. J Electrochem Soc 2005; 152:A1398–408.
[82] Jiang SP, Leng YJ, Chan SH, Khor KA. Development of (La, Sr) MnO_3-based cathodes for intermediate temperature solid oxide fuel cells. Electrochem Solid State Lett 2003;6:A67–70.
[83] Jiang SP, Chen XJ, Chan SH, Kwok JT. GDC-impregnated, $(La_{0.75}Sr_{0.25})(Cr_{0.5}Mn_{0.5})$O-3 anodes for direct utilization of methane in solid oxide fuel cells. J Electrochem Soc 2006; 153:A850–6.
[84] Wang W, Jiang SP, Tok AIY, Luo L. GDC-impregnated Ni anodes for direct utilization of methane in solid oxide fuel cells. J Power Sources 2006;159:68–72.
[85] Jiang SP, Ye YM, He TM, Ho SB. Nanostructured palladium-$La_{0.75}Sr_{0.25}Cr_{0.5}Mn_{0.5}O_3$/$Y_2O_3$-$ZrO_2$ composite anodes for direct methane and ethanol solid oxide fuel cells. J Power Sources 2008;185:179–82.
[86] Chen J, Liang FL, Liu LN, Jiang SP, Chi B, Pu J, et al. Nano-structured (La, Sr)(Co, Fe)O-3 + YSZ composite cathodes for intermediate temperature solid oxide fuel cells. J Power Sources 2008;183:586–9.
[87] Ye YM, He TM, Li Y, Tang EH, Reitz TL, Jiang SP. Pd-promoted $La_{0.75}Sr_{0.25}Cr_{0.5}Mn_{0.5}O_3$/YSZ composite anodes for direct utilization of methane in SOFCs. J Electrochem Soc 2008;155:B811–8.
[88] Babaei A, Zhang L, Tan SL, Jiang SP. Pd-promoted (La, Ca)(Cr, Mn)O-3/GDC anode for hydrogen and methane oxidation reactions of solid oxide fuel cells. Solid State Ionics 2010; 181:1221–8.
[89] Ai N, Jiang SP, Lu Z, Chen KF, Su WH. Nanostructured (Ba, Sr)(Co, Fe)O_3-delta impregnated (La, Sr)MnO_3 cathode for intermediate-temperature solid oxide fuel cells. J Electrochem Soc 2010;157:B1033–9.
[90] Chen J, Liang FL, Chi B, Pu J, Jiang SP, Jian L. Palladium and ceria infiltrated $La_{0.8}Sr_{0.2}Co_{0.5}Fe_{0.5}O_3$-delta cathodes of solid oxide fuel cells. J Power Sources 2009;194:275–80.
[91] Babaei A, Jiang SP, Li J. Electrocatalytic promotion of palladium nanoparticles on hydrogen oxidation on Ni/GDC anodes of SOFCs via spillover. J Electrochem Soc 2009;156: B1022–9.
[92] Liang FL, Chen J, Jiang SP, Chi B, Pu J, Jian L. Development of nanostructured and palladium promoted (La, Sr)MnO_3-based cathodes for intermediate-temperature SOFCs. Electrochem Solid State Lett 2008;11:B213–6.
[93] Zhao F, Zhang L, Jiang ZY, Xia CR, Chen FL. A high performance intermediate-temperature solid oxide fuel cell using impregnated $La_{0.6}Sr_{0.4}CoO_3$-delta cathode. J Alloy Compd 2009;487:781–5.
[94] Liu Y, Mori M, Funahashi Y, Fujishiro Y, Hirano A. Development of micro-tubular SOFCs with an improved performance via nano-Ag impregnation for intermediate temperature operation. Electrochem Commun 2007;9: 1918–23.
[95] Kim G, Lee S, Shin JY, Corre G, Irvine JTS, Vohs JM, et al. Investigation of the structural and catalytic requirements for high-performance SOFC anodes formed by infiltration of LSCM. Electrochem Solid State Lett 2009;12:B48–52.
[96] Shah M, Barnett SA. Solid oxide fuel cell cathodes by infiltration of $La_{0.6}Sr_{0.4}Co_{0.2}Fe_{0.8}O_3$-(delta) into Gd-doped ceria. Solid State Ionics 2008;179:2059–64.
[97] Armstrong TJ, Rich JG. Anode-supported solid oxide fuel cells with $La_{0.6}Sr_{0.4}CoO_3$-lambda-$Zr_{0.84}Y_{0.16}O_2$-delta composite cathodes fabricated by an infiltration method. J Electrochem Soc 2006;153:A515–20.
[98] Jiang ZY, Zhang L, Cai LL, Xia CR. Bismuth oxide-coated (La, Sr)MnO_3 cathodes for intermediate temperature solid oxide fuel cells with yttria-stabilized zirconia electrolytes. Electrochim Acta 2009;54:3059–65.
[99] Jiang ZY, Zhang L, Feng K, Xia CR. Nanoscale bismuth oxide im, regnated (La, Sr)MnO_3 cathodes for intermediate-temperature solid oxide fuel cells. J Power Sources 2008;185: 40–8.
[100] Chen KF, Ai N, Jiang SP. Development of (Gd, Ce)O-2-impregnated (La, Sr)MnO_3 anodes of high temperature solid oxide electrolysis cells. J Electrochem Soc 2010;157:P89–94.
[101] Yang CH, Jin C, Coffin A, Chen FL. Characterization of infiltrated $(La_{0.75}Sr_{0.25})(0.95)MnO_3$ as oxygen electrode for solid oxide electrolysis cells. Int J Hydrog Energy 2010;35: 5187–93.
[102] Tucker MC, Lau GY, Jacobson CP, DeJonghe LC, Visco SJ. Performance of metal-supported SOFCs with infiltrated electrodes. J Power Sources 2007;171:477–82.
[103] Zhang CM, Lin Y, Ran R, Shao ZP. Improving single-chamber performance of an anode-supported SOFC by impregnating anode with active nickel catalyst. Int J Hydrog Energy 2010; 35:8171–6.
[104] Zhu X, Lue Z, Wei B, Zhang Y, Huang X, Su W. Fabrication and evaluation of a Ni/La(0.75)Sr(0.25)Cr(0.5)Fe(0.5)O(3-delta) co-impregnated yttria-stabilized zirconia anode for

single-chamber solid oxide fuel cells. Int J Hydrog Energy 2010;35:6897–904.
[105] Jiang SP, Wang W. Novel structured mixed ionic and electronic conducting cathodes of solid oxide fuel cells. Solid State Ionics 2005;176:1351–7.
[106] Jiang SP, Zhang JP, Foger K. Deposition of chromium species at Sr-doped $LaMnO_3$ electrodes in solid oxide fuel cells - II. Effect on O-2 reduction reaction. J Electrochem Soc 2000; 147:3195–205.
[107] Huang YY, Ahn K, Vohs JM, Gorte RJ. Characterization of Sr-doped $LaCoO_3$-YSZ composites prepared by impregnation methods. J Electrochem Soc 2004;151:A1592–7.
[108] Zhang H, Zhao F, Chen F, Xia C. Nano-structured Sm(0.5)Sr(0.5) CoO(3-delta) electrodes for intermediate-temperature SOFCs with zirconia electrolytes. Solid State Ionics 2011;192:591–4.
[109] Choi S, Yoo S, Shin J-Y, Kim G. High performance SOFC cathode prepared by infiltration of La(n) (+) (1)Ni(n)O(3n) (+) (1) (n = 1, 2, and 3) in porous YSZ. J Electrochem Soc 2011; 158:B995–9.
[110] Liu Z, Zheng ZW, Han MF, Liu ML. High performance solid oxide fuel cells based on tri-layer yttria-stabilized zirconia by low temperature sintering process. J Power Sources 2010; 195:7230–3.
[111] Kim H, da Rosa C, Boaro M, Vohs JM, Gorte RJ. Fabrication of highly porous yttria-stabilized zirconia by acid leaching nickel from a nickel-yttria-stabilized zirconia cermet. J Am Ceram Soc 2002;85:1473–6.
[112] Kim H, Lu C, Worrell WL, Vohs JM, Gorte RJ. Cu–Ni cermet anodes for direct oxidation of methane in solid-oxide fuel cells. J Electrochem Soc 2002;149:A247–50.
[113] Jiang SP, Zhang S, Da Zhen Y, Wang W. Fabrication and performance of impregnated Ni anodes of solid oxide fuel cells. J Am Ceram Soc 2005;88:1779–85.
[114] Jiang SP, Chen XJ, Chan SH, Kwok JT, Khor KA. ($La_{0.75}Sr_{0.25}$)($Cr_{0.5}Mn_{0.5}$)O-3/YSZ composite anodes for methane oxidation reaction in solid oxide fuel cells. Solid State Ionics 2006;177:149–57.
[115] Ni M, Leung MKH, Leung DYC. Technological development of hydrogen production by solid oxide electrolyzer cell (SOEC). Int J Hydrog Energy 2008;33:2337–54.
[116] Elangovan S, Hartvigsen J, Zhao F, Bay I, Larsen D. Materials development for solid oxide electrolysis cells, in fuel cell seminar & expositions. CA: Palm Springs; 2009. p. 332–3.
[117] Liang F, Chen J, Jiang SP, Chi B, Pu J, Jian L. High performance solid oxide fuel cells with electrocatalytically enhanced (La, Sr)MnO(3) cathodes. Electrochem Commun 2009;11:1048–51.
[118] Liang F, Zhou W, Chi B, Pu J, Jiang SP, Jian L. Pd-YSZ composite cathodes for oxygen reduction reaction of intermediate-temperature solid oxide fuel cells. Int J Hydrog Energy 2011;36:7670–6.
[119] Kim J-S, Wieder NL, Abraham AJ, Cargnello M, Fornasiero P, Gorte RJ, et al. Highly active and thermally stable core-shell catalysts for solid oxide fuel cells. J Electrochem Soc 2011; 158:B596–600.
[120] He HP, Huang YY, Regal J, Boaro M, Vohs JM, Gorte RJ. Low-temperature fabrication of oxide composites for solid-oxide fuel cells. J Am Ceram Soc 2004;87:331–6.
[121] Boaro M, Vohs JM, Gorte RJ. Synthesis of highly porous yttria-stabilized zirconia by tape-casting methods. J Am Ceram Soc 2003;86:395–400.
[122] Kuengas R, Kim J-S, Vohs JM, Gorte RJ. Restructuring porous YSZ by treatment in hydrofluoric acid for use in SOFC cathodes. J Am Ceram Soc 2011;94:2220–4.
[123] Zhu W, Ding D, Xia C. Enhancement in three-phase boundary of SOFC electrodes by an ion impregnation method: a modeling comparison. Electrochem Solid State Lett 2008;11:B83–6.
[124] Nicholas JD, Barnett SA. Finite-Element modeling of Idealized infiltrated composite solid oxide fuel cell cathodes. J Electrochem Soc 2009;156:B458–64.
[125] Shah M, Nicholas JD, Barnett SA. Prediction of infiltrated solid oxide fuel cell cathode polarization resistance. Electrochem Commun 2009;11:2–5.
[126] Jiang SP, Love JG, Ramprakash Y. Electrode behaviour at (La, Sr)MnO_3/Y_2O_3-ZrO_2 interface by electrochemical impedance spectroscopy. J Power Sources 2002;110:201–8.
[127] Steele BCH. Appraisal of Ce1-y$GdyO_2$-y/2 electrolytes for IT-SOFC operation at 500 °C. Solid State Ionics 2000;129: 95–110.
[128] Jiang SP, Wang W. Effect of polarization on the interface between (La, Sr) MnO_3 electrode and Y_2O_3-ZrO_2 electrolyte. Electrochemical Solid State Lett 2005;8:A115–8.
[129] Liang FL, Chen J, Chi B, Pu JA, Jiang SP, Jian L. Redox behavior of supported Pd particles and its effect on oxygen reduction reaction in intermediate temperature solid oxide fuel cells. J Power Sources 2011;196:153–8.
[130] Fox EB, Lee AF, Wilson K, Song CS. In-situ XPS study on the reducibility of Pd-promoted Cu/CeO_2 catalysts for the oxygen-assisted water-gas-shift reaction. Top Catal 2008;49: 89–96.
[131] Nabae Y, Yamanaka I. Alloying effects of Pd and Ni on the catalysis of the oxidation of dry CH_4 in solid oxide fuel cells. Appl Catal A-Gen 2009;369:119–24.
[132] Ralph JM, Schoeler AC, Krumpelt M. Materials for lower temperature solid oxide fuel cells. J Mater Sci 2001;36: 1161–72.
[133] Wang SZ, Zhong H. High performance Pd promoted $Sm_{0.5}Sr_{0.5}CoO_3$-$La_{0.8}Sr_{0.2}Ga_{0.8}Mg_{0.15}Co_{0.05}O_3$-delta composite cathodes for intermediate temperature solid oxide fuel cells. J Power Sources 2007;165:58–64.
[134] Serra JM, Buchkremer HP. On the nanostructuring and catalytic promotion of intermediate temperature solid oxide fuel cell (IT-SOFC) cathodes. J Power Sources 2007;172: 768–74.
[135] Bidrawn F, Kim G, Aramrueang N, Vohs JM, Gorte RJ. Dopants to enhance SOFC cathodes based on Sr-doped LaFeO(3) and LaMnO(3). J Power Sources 2010;195:720–8.
[136] Yamahara K, Jacobson CP, Visco SJ, De Jonghe LC. Catalyst-infiltrated supporting cathode for thin-film SOFCs. Solid State Ionics 2005;176:451–6.
[137] Huang YY, Vohs JM, Gorte RJ. An examination of LSM-LSCo mixtures for use in SOFC cathodes. J Electrochem Soc 2006; 153:A951–5.
[138] Imanishi N, Ohno R, Murata K, Hirano A, Takeda Y, Yamamoto O, et al. LSM-YSZ cathode with infiltrated cobalt oxide and cerium oxide nanoparticles. Fuel Cells 2009;9: 215–21.
[139] Haanappel VAC, Rutenbeck D, Mai A, Uhlenbruck S, Sebold D, Wesemeyer H, et al. The influence of noble-metal-containing cathodes on the electrochemical performance of anode-supported SOFCs. J Power Sources 2004;130:119–28.
[140] Hansen KK, Wandel M, Liu YL, Mogensen M. Effect of impregnation of La(0.85)Sr(0.15)MnO(3)/yttria stabilized zirconia solid oxide fuel cell cathodes with La(0.85)Sr(0.15) MnO(3) or Al(2)O(3) nano-particles. Electrochim Acta 2010; 55:4606–9.
[141] Lee S, Miller N, Abernathy H, Gerdes K, Manivannan A. Effect of Sr-doped LaCoO(3) and LaZrO(3) infiltration on the performance of SDC-LSCF cathode. J Electrochem Soc 2011; 158:B735–42.
[142] Lynch ME, Yang L, Qin W, Choi J-J, Liu M, Blinn K, et al. Enhancement of La(0.6)Sr(0.4)Co(0.2)Fe(0.8)O(3-delta) durability and surface electrocatalytic activity by La(0.85) Sr(0.15)MnO(3+/-delta) investigated using a new test electrode platform. Energy Environ Sci 2011;4:2249–58.

[143] Choi Y, Lin MC, Liu M. Rational design of novel cathode materials in solid oxide fuel cells using first-principles simulations. J Power Sources 2010;195:1441–5.
[144] Liu Y, Hashimoto S, Yasumoto K, Takei K, Mori M, Funahashi Y, et al. Preparation and application of nano-dispersed Ag in $La_{0.6}Sr_{0.4}CoxFe1\text{-}xO_3$-delta perovskites for intermediate-temperature solid oxide fuel cell. Curr Appl Phys 2009;9:S51–3.
[145] Hojberg J, Sogaard M. Impregnation of LSM based cathodes for solid oxide fuel cells. Electrochem Solid State Lett 2011; 14:B77–9.
[146] Chen J, Liang FL, Yan D, Pu J, Chi B, Jiang SP, et al. Performance of large-scale anode-supported solid oxide fuel cells with impregnated $La_{0.6}Sr_{0.4}Co_{0.2}Fe_{0.8}O_3$-delta+$Y_2O_3$ stabilized ZrO_2 composite cathodes. J Power Sources 2010;195:5201–5.
[147] Horita T, Kishimoto H, Yamaji K, Brito ME, Xiong YP, Yokokawa H, et al. Effects of impurities on the degradation and long-term stability for solid oxide fuel cells. J Power Sources 2009;193:194–8.
[148] Lu XC, Zhu JH, Yang ZG, Xia GG, Stevenson JW. Pd-impregnated SYT/LDC composite as sulfur-tolerant anode for solid oxide fuel cells. J Power Sources 2009;192:381–4.
[149] Zhen YD, Jiang SP. Transition behavior for O-2 reduction reaction on (La, Sr)MnO_3/YSZ composite cathodes of solid oxide fuel cells. J Electrochem Soc 2006;153:A2245–54.
[150] Shah M, Voorhees PW, Barnett SA. Time-dependent performance changes in LSCF-infiltrated SOFC cathodes: the role of nano-particle coarsening. Solid State Ionics 2011; 187:64–7.
[151] Wang W, Gross MD, Vohs JM, Gorte RJ. The stability of LSF-YSZ electrodes prepared by infiltration. J Electrochem Soc 2007;154:B439–45.
[152] Liang FL, Chen J, Jiang SP, Wang FZ, Chi B, Pu J, et al. Mn-stabilised microstructure and performance of Pd-impregnated YSZ cathode for intermediate temperature solid oxide fuel cells. Fuel Cells 2009;9:636–42.
[153] Babaei A, Zhang L, Liu EJ, Jiang SP. Performance and stability of La(0.8)Sr(0.2)MnO(3) cathode promoted with palladium based catalysts in solid oxide fuel cells. J Alloy Compd 2011; 509:4781–7.
[154] Zhao F, Peng RR, Xia CR. A $La_{0.6}Sr_{0.4}CoO_3$-delta-based electrode wit high durability for intermediate temperature solid oxide fuel cells. Mater Res Bull 2008;43:370–6.
[155] Zhang YX, Xia CR. A durability model for solid oxide fuel cell electrodes in thermal cycle processes. J Power Sources 2010;195:6611–8.
[156] Busawon AN, Sarantaridis D, Atkinson A. Ni infiltration as a possible solution to the redox problem of SOFC anodes. Electrochem Solid State Lett 2008;11:B186–9.
[157] Jiang SP. Activation, microstructure, and polarization of solid oxide fuel cell cathodes. J Solid State Electrochem 2007;11:93–102.
[158] Leng YJ, Chan SH, Khor KA, Jiang SP. Development of LSM/YSZ composite cathode for anode-supported solid oxide fuel cells. J Appl Electrochem 2004;34:409–15.
[159] Jiang SP, Love JG. Origin of the initial polarization behavior of Sr-doped $LaMnO_3$ for O-2 reduction in solid oxide fuel cells. Solid State Ionics 2001;138:183–90.
[160] Backhaus-Ricoult M, Adib K, Clair TS, Luerssen B, Gregoratti L, Barinov A. In-situ study of operating SOFC LSM/YSZ cathodes under polarization by photoelectron microscopy. Solid State Ionics 2008;179:891–5.
[161] Kim J-S, Lee S, Gorte RJ, Vohs JM. Substrate-mediated spreading and phase segregation at LSM-zirconia interfaces. J Electrochem Soc 2011;158:B79–83.
[162] Bidrawn F, Kuengas R, Vohs JM, Gorte RJ. Modeling impedance response of SOFC cathodes prepared by infiltration. J Electrochem Soc 2011;158:B514–25.